Originally published 21 June 2018; corrected 9 July 2018

www.sciencemag.org/cgi/content/full/science.aar4199/DC1

Supplementary Materials for

Mediator and RNA polymerase II clusters associate in transcription-dependent condensates

Won-Ki Cho*, Jan-Hendrik Spille*, Micca Hecht, Choongman Lee, Charles Li, Valentin Grube, Ibrahim I. Cisse†

*These authors contributed equally to this work.
†Corresponding author. Email: icisse@mit.edu

Published 21 June 2018 on *Science* First Release
DOI: 10.1126/science.aar4199

This PDF file includes:

Other Supplementary Material for this manuscript includes the following:
(available at www.sciencemag.org/cgi/content/full/science.aar4199/DC1)

Movies S1 to S3

Correction: Since First Release, the *y*-axis label in fig. S5B has been corrected to refer to Pol II rather than Mediator, and minor editorial changes have been made in the legends to figs. S6 and S9.

Materials and Methods

Mouse embryonic stem cell (mESC) culture

Mouse embryonic stem cells (mESCs) (R1 ES cells) were cultured in serum-free 2i media (1:1 of DMEM/F-12 and Neurobasal media, supplemented with 1x N-2 supplement, 1x B-27 supplement, 100 U/ml PenStrep, 3 μg/ml AlbuMAX™ II, 1x MEM NEAA, 1mM Sodium pyruvate, 1mM L-glutamine (all from Thermo Fisher Scientific), 0.1 μM 2-Mercaptoethanol (Sigma-Aldrich), 1mM MEK inhibitor (PD0325910, Stemgent), 3mM GSK3β inhibitor (CHIR99021, Stemgent) and 100 U/ml LIF (Leukemia Inhibitory Factor, EMD Millipore) without feeder cells). Prior to cell culturing, all the flasks or petri dishes were incubated in 37°C for more than 5 hours with 5 μg/ml poly-L-ornithine (PLO, Sigma) in 1x PBS buffer, followed by 5 μg/ml Laminin (VWR) in 1x PBS buffer with >5 hours incubation in 37°C. The cells were grown in a 37°C incubator maintaining 5% CO2 in a water-saturated atmosphere. Cell culture media were exchanged every 24 hours. Pluripotency of mESC was checked periodically by alkaline phosphatase (AP) expression level using Alkaline Phosphatase Live Stain Kit (Thermo Fisher Scientific), and by cell phenotype. Note that stem cell-specific large/stable Pol II and Mediator clusters may also serve as stemness markers.

Homology-directed repair (HDR) DNA template design

Plasmids containing Dendra2-*Rpb1* and Dendra2-*Med19* DNA repair templates were synthesized with long homology arms (~500 bp) by GeneArt® Gene Synthesis (Life Technologies, Carlsbad, CA). Silent mutations were included in the repair template design to mask the sgRNA target sites and avoid Cas9 degradation of the repair templates. Repair templates were linearized by PCR using primers listed in **Table S2**. Left homology arm (LHA) and right homology arm (RHA) sequences were designed from the mouse *Rpb1* gene (ENSMUSG00000005198) covering distances of 427 bp and 314 bp respectively from each side of the ATG start codon of *Rpb1*. The Dendra2 (*31*) sequence (690 bp) was inserted between these homology arms to fuse Dendra2 with the N-terminus of the Rpb1 protein. The same strategy was applied to target the mouse *Med19* gene (ENSMUSG00000027080) with 301 bp LHA and 207 bp RHA sequences flanking Dendra2, which lies in-frame with the ATG start codon of *Med19*.

To generate a Halo-*Med19* repair template, HaloTag was inserted in place of Dendra2 in the Dendra2-*Med19* plasmid using the Gibson Assembly® Ultra Kit from SGI-DNA. Prior to assembly, the Dendra2-*Med19* plasmid was linearized by PCR to form a vector omitting the Dendra2 sequence and with ~20 bp overhangs for HaloTag insertion. The HaloTag insert was amplified by PCR from pENTR4-HaloTag (w876-1) using primers that provide a 40 bp overlap with each end of the destination vector. Gibson primers are listed in **Table S3**.

To replace Dendra2 in the Dendra2-*Rpb1* repair template and create the Halo-*Rpb1* repair template we used *AarI* (Thermo Fisher) and PCR to create sequence-independent sticky ends between the HaloTag insert and the *Rpb1* backbone. **Table S4** lists PCR primers used to generate compatible fragments from pENTR4-HaloTag and Dendra2-*Rpb1* repair template. *AarI* digestion of the two PCR products, and ligation with T7 Ligase (NEB), produced the Halo-*Rpb1* repair template plasmid. pENTR4-HaloTag

(w876-1) was a gift from Eric Campeau (Addgene plasmid # 29644). *AarI* and *BbsI* were obtained from Thermo Fisher. All other restriction enzymes were obtained from NEB.

CRISPR/Cas9 engineering for endogenous Pol II and Mediator labeling

Single-guide RNAs (sgRNAs) targeting +/- 100 bps from the start codons of the *Rbp1* and *Med19* genes were designed using the web-based CRISPR Design tool (http://crispr.mit.edu). Three sgRNAs were selected for each target (**Table S1**). DNA oligonucleotides for sgRNAs with *BbsI* restriction sites were obtained from Integrated DNA Technologies (IDT). *Streptococcus pyogenes* Cas9 vectors (pSpCas9(BB)-2A-Puro (PX459) V2.0, Addgene #62988) and DNA oligonucleotides were digested using *BbsI* enzyme (Thermo Fisher) and ligated to form sgRNA-Cas9 plasmids. These plasmids were transformed into *Stbl3* competent cells (Life Technologies) and sequence-verified. pSpCas9 (BB)-2A-Puro (PX459) V2.0 was a gift from Feng Zhang (Addgene plasmid #62988).

700 ng sgRNA-Cas9 plasmids and 2 μg repair template DNA were electroporated to 1-2 million cells using 4D Nucleofector X Unit (Lonza) with P3 Primary Cell Nucleofection Kit (Lonza). Cells were plated to 6-well plates in recovery buffer (2i, supplemented with 2-5% FBS). After 2 hour incubation, recovery buffer was replaced by 2i media. Note that among three sgRNAs for each gene, sgRNA #2 for *Rpb1* and sgRNA #1 for *Med19* were most successful for CRISPR/Cas9 gene editing.

In a first step we generated monoclonal cell lines expressing either Dendra2-Rpb1 or Dendra2-Med19. In a second step, we added the orthogonal label to generate monoclonal Dendra2-Rpb1/Halo-Med19 and Dendra2-Med19/Halo-Rpb1 cell lines.

Flow cytometric cell sorting using fluorescence-activated cell sorting (FACS)

Within 48-72 hours after co-transfection with sgRNA-Cas9 plasmids and repair templates, the cells were tested on the microscope stage to confirm successful CRISPR/Cas9 gene editing. For Dendra2-fused cells 488-nm illumination was used, and for Halo-fused cells 642-nm illumination was used after 20 min incubation with 100nM JF646-Halotag ligand (*13*). Fluorescence signal from the nucleus in a small fraction of cells confirmed successful gene editing. To create monoclonal cell lines, fluorescence-activated cell sorting (FACS) was utilized. For FACS preparation, the cells were centrifuged to discard 2i media, resuspended in FACS buffer (25mM HEPES (pH7.4), 1mM EDTA, 1% FBS in 1x PBS buffer), then strained through a 35 μm sieve (Falcon, #2235).

Cells were sorted using BD FACS Aria I at the Koch Institute Flow Cytometry Core at MIT. Fluorescence-positive cells were sorted into PLO/Laminin-coated 96-well plates. The cell lines without CRISPR/Cas9 gene editing were used as negative controls for FACS. Sorted cells were grown in recovery buffer (2i, supplemented with 2-5% FBS) for 6 hours before the buffer was replaced by regular 2i media.

Stable Expression of NLS-MCP-SNAP in ES cell lines

In order to visualize MS2 stem loops engineered into endogenous transcripts, we generated cells stably expressing the MS2 capsid protein (MCP) fused to a SNAP-Tag moiety by incubating cells with a newly cloned EF1α-NLS-MCP-SNAP expression vector. The SNAP sequence was amplified from pENTR4-SNAPf (Addgene plasmid

#29652) using primers listed in **Table S5**, then digested with *AarI*. The vector was generated by digesting phage-Ubc-NLS-2xMCP-Halo (Addgene plasmid #64540) with *NotI* and *Xba*I to remove Halo and replace it with the SNAP DNA sequence. The 2xMCP-SNAP sequence was then digested with *NotI* and *BsrGI* and inserted into the backbone of pDendra2-C (Clontech) with an *AarI* placeholder for cloning a new promoter. The *AarI* placeholder was generated by annealing two oligonucleotides to form *PciI* and *NotI* overhangs (**Table S5**). The human elongation factor 1 alpha promoter (EF1α) was chosen for improved stability in mESC. By digesting pDendra2-C with *PciI* and *BsrGI*, we removed the CMV promoter and Dendra2 in order to replace these with EF1α and 2xMCP-SNAP. When digested with *AarI*, the placeholder exposes sticky ends compatible with insertion of an EF1α promoter sequence, which was obtained from pHAGE-EFS-MCP-3XBFPnls (Addgene #75384) through double-digestion with *NheI* and *MluI*. Intermediate and final ligation products were transformed into Subcloning Efficiency *DH5*α Competent Cells (Life Technologies) and confirmed by Sanger Sequencing before transfection. The plasmids used for cloning EF1α-NLS-MCP-SNAP are listed in **Table S6**.

EF1α-NLS-MCP-SNAP was then transfected into the Dendra2-Rpb1/Halo-Med19 cell line using 4D Nucleofector X Unit (Lonza) with P3 Primary Cell Nucleofection Kit (Lonza). 3 days after transfection, cells were incubated with 100 nM JF646-SNAPtag ligand for 20 min and washed three times. Single cells with positive signals were sorted into 96-well plates by FACS. Two weeks after FACS, sorted single cells were incubated with 100 nM JF646-SNAPtag ligands again to be tested on the microscope stage. Under 642-nm illumination, only cells with stable fluorescence signals from JF646 in the nucleus were selected to grow a Dendra2-Rpb1/Halo-Med19/MCP-SNAP cell line.

Generating Esrrb-T2A-PuroR-24xMS2 Cell Line

Starting with the previously engineered Dendra2-Rpb1/Halo-Med19/MCP-SNAP cell line, a repetitive DNA region encoding 24 MS2 stem loop repeats (24xMS2) was knocked into the 3´ untranslated region (UTR) of the endogenous mouse Estrogen-related receptor beta gene (*Esrrb*) using a CRISPR sgRNA that cleaves immediately before the TGA stop codon of endogenous *Esrrb* in exon 7 (ENSMUSG00000021255). The guide sequence (**Table S1**) was inserted into pSpCas9 (BB)-2A-Puro(PX459)V2.0 as described above. The sgRNA-Cas9 plasmid was co-transfected with a circular repair plasmid containing homology arms of 800 base-pairs on either side of the *Esrrb* stop codon. For selection of cells edited to express the 24xMS2 sequence we inserted a T2A-*PuroR*-24xMS2 cassette between the homology arms.

The repair plasmid was derived from a minimal mammalian expression vector (GeneArt® Gene Synthesis, Life Technologies, Carlsbad, CA) that served as the initial destination vector for the *Esrrb* repair template. The backbone was linearized by PCR, using long primers with *AarI* sites for insertion of a synthetic gene block (AarI-gblock-v2) in order to introduce multiple cloning sites into the initial destination vector. The primers used for backbone amplification and the full AarI-gblock-v2 sequence are listed in **Table S5**. Two inverted *AarI* sites flanked by *Esrrb* LHA and RHA were synthesized as a single gene block (Genewiz FragmenGENE Synthesis), which was cloned into the initial destination vector using restriction enzymes *MfeI* and *MluI* to create an intermediate destination vector. A donor plasmid encoding self-cleaving peptide T2A and

a Puromycin-resistance gene (*PuroR*) was created separately by PCR amplification of *PuroR* from pCRISPaint-HaloTag-*PuroR (*Addgene plasmid # 80960), with primers encoding the T2A sequence (**Table S5**), as well as *EagI* and *BamHI* restriction sites for insertion into pDZ415 (24MS2SL loxP-Kan-loxP) (Addgene plasmid # 45162). The resulting donor plasmid containing T2A-*PuroR*-24xMS2 was digested with *EagI* and *SalI* to produce restriction overhangs compatible with *AarI* digestion and T7 ligation into the *Esrrb* destination vector. The final *Esrrb-MS2* HDR plasmid was transformed into *Stbl3* competent cells and verified by Sanger Sequencing prior to transfection. The plasmids used for cloning the *Esrrb-MS2* HDR plasmid are listed in **Table S6.**

PCR genotyping

Sorted cells were cultured as distinct monoclonal cell lines. Genomic DNA from each cell line was isolated using GeneElute™ Mammalian Genomic DNA Miniprep Kits from Sigma-Aldrich (St. Louis, MO). To test the cells for Dendra2 and HaloTag insertion, PCR primers were designed to amplify the targeted gene loci as well as the 5'- and 3'-junctions between the desired insert and left or right homology arms (j5 and j3 respectively as in **Table S7, Table S8,** and **Table S9**). To check the 3'UTR of *Esrrb* for successful knock-in of the T2A-*PuroR*-24xMS2 transgene, PCR junctions j5 and j3 were designed to amplify the junctions between homology arms and the transgenic cassette, while avoiding the repetitive array of MS2 stem loops. PCR products were analyzed on 1% agarose gels (**Fig. S2 and S15**). Gel fragments were extracted using Monarch® Nucleic Acid Purification Kits (NEB) before submission to Genewiz for Sanger Sequencing. Alignment of the DNA sequences confirmed integration of Dendra2 or HaloTag in *Med19* and *Rpb1*, respectively, in Halo-*Rpb1*/Dendra2-*Med19* and Dendra2-*Rpb1*/HaloTag-*Med19* cell lines. Sequencing results are summarized in **Fig. S2 and S15** and **Tables S10**.

Differentiation to epiblast-like cells (EpiLC)

Prior to EpiLC differentiation induction, mESC were cultured in 2i media at least for two passages from frozen stocks. After washing with PBS and sieving with a 70μm cell strainer (Corning Falcon), mESC were transferred to either 6-well plates for qRT-PCR or glass-bottom dishes for fluorescence imaging, in N2B27-based medium supplemented with 1% KOSR (Invitrogen) and 12 mg/ml bFGF (Peprotech). Dishes and plates were coated with 5 μg/mL Fibronectin (*16*).

JQ1, DRB, hexanediol treatment

Cells were plated on glass-bottom dishes and maintained in 2i media until a confluency of >50% was reached. For JQ1 treatment, 500 nM-5 μM JQ1 (Sigma-Aldrich, SML0974) were added to 2i media and maintained for 24 hours before imaging.

For DRB (5,6-Dichloro-1-beta-D-ribofuranosyl-benzimidazole) treatment, 100-200μM DRB (Sigma-Aldrich, D1916) was added to L-15 medium (*32*). For DRB washing experiments, DRB buffer was exchanged with L-15 medium after gently washing the dishes three times with 37°C 1x PBS or L-15 medium.

For hexanediol treatment cells were imaged in 500μl L-15 medium. We prepared a stock solution of 20% (v/v) hexanediol in L-15 and carefully added 500μl of pre-warmed solution to the imaging dish on the microscope for a final concentration of 10% (v/v).

Stacks (z-range 5μm, z-spacing 400nm) of the same field of view were acquired every before addition of hexanediol, and 1, 3, 5, 7, 9, 12, and 15 min after addition. Clusters were identified in maximum intensity projections of the stacks.

Super-resolution imaging

Live cell PALM imaging was carried out as described before (*14, 15, 33*). Briefly, cells were simultaneously illuminated with 1.3 W/cm^2 near UV light (405nm) for photo-conversion of Dendra2 and 3.2 kW/cm^2 (561nm) for fluorescence detection with an exposure time of 50 ms. We acquired images of Dendra2-Mediator for 100s (2000 frames) and Dendra2-Pol II for 150s (3000 frames) for quantification of transient and stable clusters. For dual color imaging, cells were incubated with 100nM JF646 Halo ligand for 20 min and washed with 1x PBS, followed by 30 min incubation in 2i media without JF646-HaloTaq ligands, to wash out unbound HaloTaq ligands before fluorescence imaging in L-15 medium. We acquired 100 frames (5s) with 642nm excitation and quickly switched to simultaneous 405/561 imaging for PALM. Super-resolution images were reconstructed using MTT (*34*) and qSR (*35*).

Density based spatial clustering of applications with noise (DBSCAN) analysis

We use a clustering algorithm, density based spatial clustering of applications with noise (DBSCAN) (*36*), to define the area of clustered regions in super-resolution data. Based on the single molecule localization in a super-resolution image, DBSCAN tests if a localization can be grouped with nearby localizations. Once a localization has a minimum number of nearby localizations (*N*) within a specific distance (*R*), it is grouped with other localizations also satisfying *N* and *R* criteria in their local neighborhood. We defined the parameters as *N* = 15-20 (points) and *R* = 100 (nm) for Dendra2-Mediator clustering, and *N* = 25-30 (points) and *R* = 90-95 (nm) for Dendra2-Pol II clustering. Varying the parameters for an image, we chose a set of parameters (*N, R*) for which the DBSCAN-clustering result is agrees with intensified regions in the super-resolution image generated from our qSR software module (**Fig. S4**). For DBSCAN analysis, we used the 'DBSCAN' module embedded in qSR software.

Fluorescence Recovery After Photobleaching (FRAP)

FRAP experiments were performed at the W.M. Keck Microscopy Facility at the Whitehead Institute using an Andor Revolution Spinning Disk Confocal microscope with FRAPPA module. Cells were labelled with JF646 Halo ligand as described above. Images of a single confocal plane were taken with an exposure time of 200 ms. The bleach spot was centered on a cluster and images were taken with 1s interval for 1min to measure the fluorescence recovery in the cluster. To quantify FRAP recovery we followed the approach described by Darzacq et al. (*37*). Briefly, we determined the integrated intensity of the cluster as a function of time, subtracted background intensity from a neighboring region of equal size, corrected for overall photo-bleaching based on a reference region within the same cell, and normalized to pre-bleach intensity. We averaged normalized traces and fitted the recovery with a single exponential recovery model $I(t) = A \cdot (1 - \exp(-t/\tau))$, where A denotes the recovery fraction and τ is the mean recovery time.

Lattice Light Sheet Microscopy

We built a lattice light sheet microscope under license from HHMI, Janelia Research Campus as described in (*10*). Cells were grown and labeled as described above, and imaged in Leibovitz's L-15 medium at 37°C for up to 3 hours. A lattice light sheet consisting of 61 Bessel beams was generated with an annulus of inner/outer numerical aperture NA 0.44/0.55. Fast tracking experiments were conducted with 25ms frame interval in a single plane and 1.2 mW laser power (642nm) measured before the excitation objective. Time-lapse imaging was conducted with 100ms exposure time and laser powers of 0.1 mW (488nm) and 0.6 mW (642nm) respectively. Cells were stepped through the light sheet to acquire stacks with 0.3μm z-spacing, resulting in a rate of 10-30s/stack. Fluorescence was detected using a quad band notch filter in front of a sCMOS camera (Orca Flash v4.2, Hamamatsu). Images were processed (deskewed) using LLSpy (*38*) and FIJI (*39*). Where appropriate we performed chromatic aberration correction by translating one of the color channels based on multi-color bead (TetraSpeck, Thermo Fisher Scientific) images. Analysis was performed using MATLAB and FIJI scripts.

Counting clusters using lattice light sheet microscopy

The number of clusters per cell was determined from maximum intensity projections of full volumetric data. To facilitate detection of dim spots we subtracted a median filtered image (radius 8 pixel) from the raw data, smoothed with a 1 pixel radius Gaussian kernel and applied a threshold to count the number of local maxima above background within a cell nucleus. Nuclear outlines were segmented manually. Counting was performed using the brighter Halo-tagged cell lines for both, Pol II and Mediator, in separate experiments (see **Fig. S6**).

Colocalization analysis

For lattice light sheet-based colocalization analysis cells were labelled with JF646-Halo-ligand as described above and fixed in 4% PFA. Stacks were acquired using 488nm illumination for direct visualization of Dendra2-labelled protein and 642nm illumination for Halo-tagged protein. We then identified clusters as described above and fitted their centroid position with a 2D Gaussian peak. To quantify colocalization of diffraction-sized signals we opted for an object-based approach. Since Dendra2 signal was weaker and dimmer clusters may not be detectable above the noise floor, we analyzed colocalization based on clusters identified in the Dendra2 channel. For each clusters in this channel we measured the distance to the nearest identified cluster in the Halo channel. Since lattice light sheet microscopy is a diffraction-limited imaging modality with a resolution of approximately half the emission wavelength (detection objective NA 1.2), we define those cluster as colocalized that were separated by less than 300nm.

We note that colocalization between PALM super-resolution images and epifluorescence images is not well-defined since both channels have different resolution and pixel sizes. Moreover, the PALM images are merely renderings of single molecule localization data. Here, we generated a rendered super-resolution image by placing Gaussian peaks with spread corresponding to the localization accuracy (50 nm) at the position of single molecule localizations. To localize JF646-Halo-cluster regions in conventional fluorescence images, we subtracted background (rolling ball with 50 pixel

radius) and adjusted the contrast to remove fluorescence background in the nucleus which is higher than background in the cytoplasm. We adjusted the size of direct images to that of super-resolution images and merged color channels in ImageJ. We then identified clusters in PALM images. These corresponded to the brightest peaks in the epi fluorescence images. Since clusters in PALM images are not well-described by a single Gaussian peak we calculated the centroid (center of mass) of a region of interest (800nm x 800nm) and determined the distance between the centroids of the PALM and epi fluorescence channels (**Fig. S9**).

Tracking clusters

Clusters were localized in maximum intensity projections using ThunderStorm (*39*) and connected to trajectories using a MATLAB script. The mean square displacement was calculated for all trajectories spanning at least 60 frames. (Fgf5 enhancer using CARGO: 23 trajectories comprising 7009 displacements in 15 cells. Clusters: 18 trajectories comprising 5452 displacements in 6 cells.). We fitted with a general model $MSD = b * \Delta t^{\alpha} + c$ in Origin to determine the scaling exponent of the mean square displacement, α (**Fig. S13**).

Nascent RNA pulse labelling

Nascent RNA was labelled using the Click-IT RNA Alexa Fluor Imaging Kit (Thermo Fisher Scientific) with a modified protocol. For pulse labelling we incubated cells with 100nM JF505 Halo-ligand and 100µM DRB in 2i medium for 20mins followed by 10mins in 100µM DRB in 2i medium without JF505 Halo-ligand. We then exchanged the medium to 2i supplemented with 2.5mM 5-ethynyl uridine (EU) for 2mins and fixed immediately in 4% PFA. For control experiments medium was exchanged to 2i with 2.5mM EU and 100µM DRB in the last step to maintain transcription inhibition. Click-labelling of EU incorporated into nascent RNA (*40*) was performed according to manufacturer instructions using AlexaFluor647 azide (Thermo Fisher Scientific).

Fixed cells were imaged on the lattice light sheet microscope. Clusters were identified in the Mediator-JF505 channel as described below. For analysis we subtracted background in both channels by median-filtering (radius 8 pxl). We extracted regions of interest centered on the cluster signal from single z planes in both, the Mediator-JF505 and the EU-AF647 channel. To further enhance visibility we averaged the signal for all regions of interest in individual cells. As a control, we randomized the cluster positions within the nucleus and performed the same type of analysis. We note that nucleoli typically show the strongest EU signal because they contain highly transcribed rDNA genes and DRB does not act on Pol I. Nucleolar regions were thus excluded from the analysis.

Fluorescent in situ hybridization (FISH)

We designed RNA FISH probes (Stellaris FISH Probes, LGC Biosearch Technologies, Novato, CA), targeting intron 3 of *Esrrb*. Probes were labeled with Quasar670. Cells were grown on 5mm round cover glasses as described above. Cells were labelled with JF549-Halo ligand as described above, washed with 37°C 1x PBS, fixed with 4% paraformaldehyde in PBS for 10 min, washed with 1x PBS three times, and permeablized in 70% ethanol for 1h at 4°C. For probe hybridization, we followed the

Stellaris protocol for adherent cells incubating with 125nM probe concentration for 3-4hrs. All samples were imaged using Lattice Light Sheet Microscopy on the day of preparation and under identical imaging conditions.

Tracking of endogenous transcription sites and clusters

For dual-color imaging of MS2-labelled gene loci and clusters we incubated cells with a mix of 100nM JF646-SNAP-ligand and JF549-Halo-ligand. Stacks were acquired with 1min interval and 100ms exposure time using laser powers of 0.05 mW (561nm) and 0.3 mW (642nm). The Esrrb transcription site was readily identified as a diffraction-limited fluorescent peak in maximum intensity projections. For further analysis we subtracted background plane-by-plane by median-filtering (8 pxl radius). The transcription site was tracked in maximum intensity projections using the ThunderSTORM ImageJ plugin (*41*), and in each frame the distance to the nearest cluster was determined.

Supplementary Figures

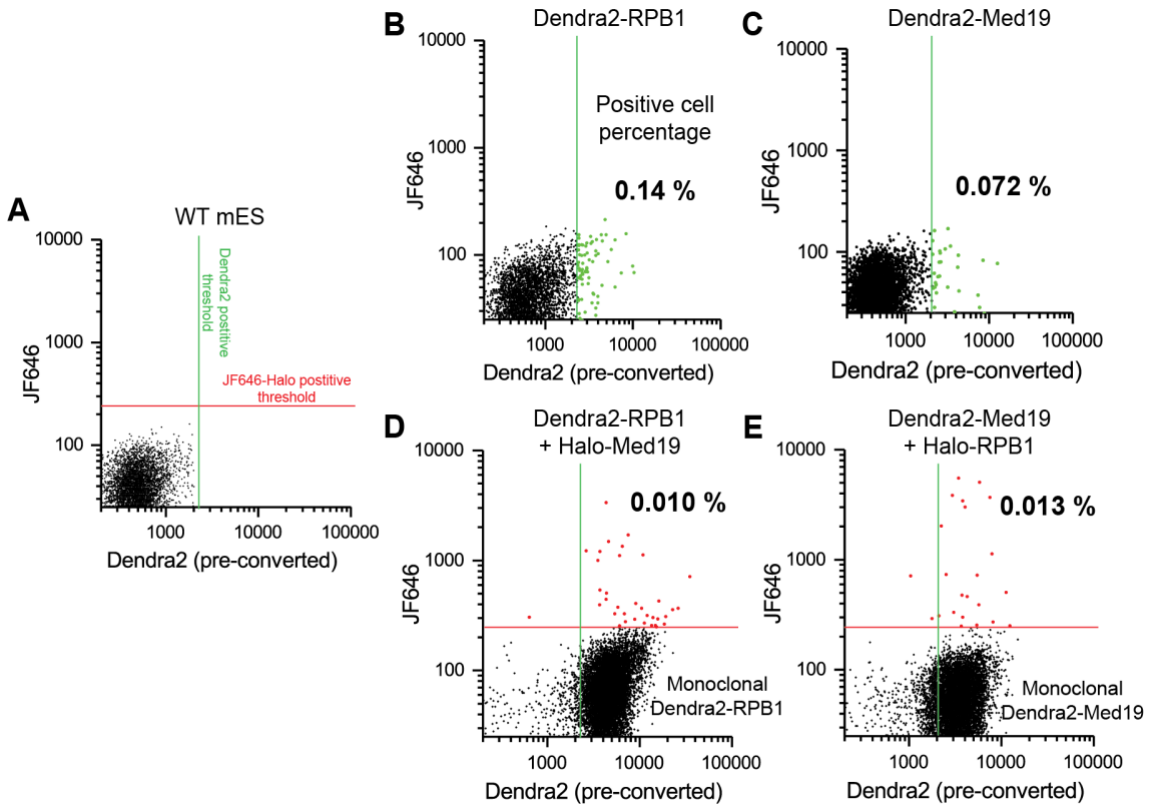

Fig. S1. CRISPR/Cas9 gene engineering for dual-color imaging

To endogenously label RNA Polymerase II (Pol II), we picked the largest subunit, *Rpb1*, as described before for mouse embryonic fibroblast cells (*33*). To label Mediator we chose *Med19* subunit, which is the largest subunit that forms the main frame of the Middle domain in the Mediator complex (*42*). To prevent functional interruption, we targeted the N-terminal domain of Med19 (*42*, *43*). Fluorescence-activated cell sorting (FACS) results of (**A**) wild type mESC, CRISPR/Cas9-engineered (**B**) Dendra2-Rpb1, (**C**) Dendra2-Med19, (**D**) Halo-Med19 on the Dendra2-Rpb1 monoclonal cell line and (**E**) Halo-Rpb1 on the Dendra2-Rpb1 monoclonal cell line. Vertical green lines indicate sorting threshold for Dendra2-positive signals with 488-nm excitation, and horizontal red lines indicate JF646-positive signals with 642-nm excitation.

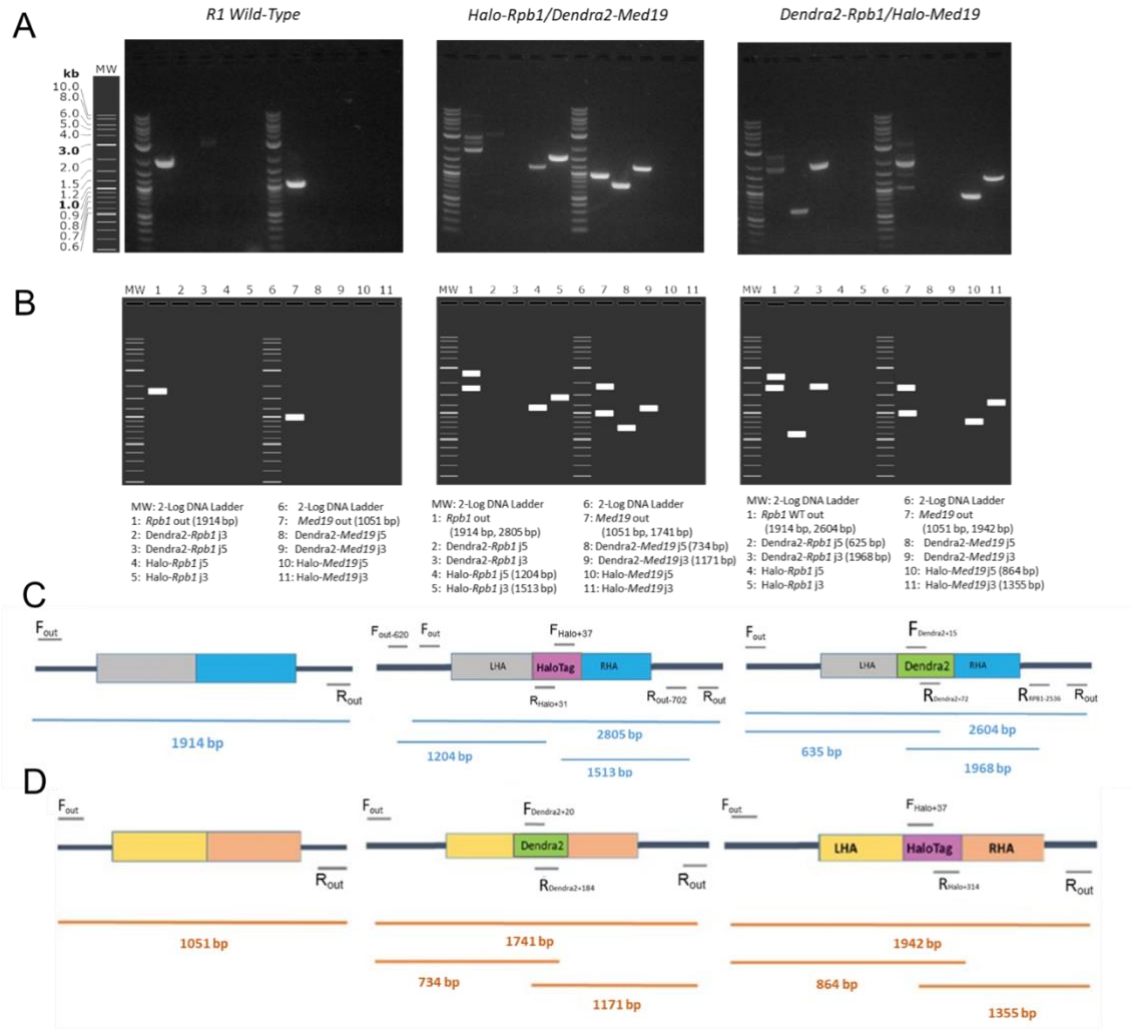

Fig. S2. CRISPR validation by PCR

(A) Genomic DNA was amplified by PCR from 3 cell lines using primers listed in **Table S7** and **S8. (B)** Expected fragments were plotted with a legend that matches lane numbers to PCR products of interest. **(C)** Corresponding PCR products are represented in context under each gene locus: WT-*Rpb1* (left), Halo-*Rpb1* (middle), and Dendra2-*Rpb1* (right) **(D)** WT-*Med19* (left), Dendra2-*Med19* (middle), Halo-*Med19* (right). For each locus, PCR products were sequenced in both directions using the generative primers, and these traces were aligned with the full-length sequence to provide a consensus across each gene target.

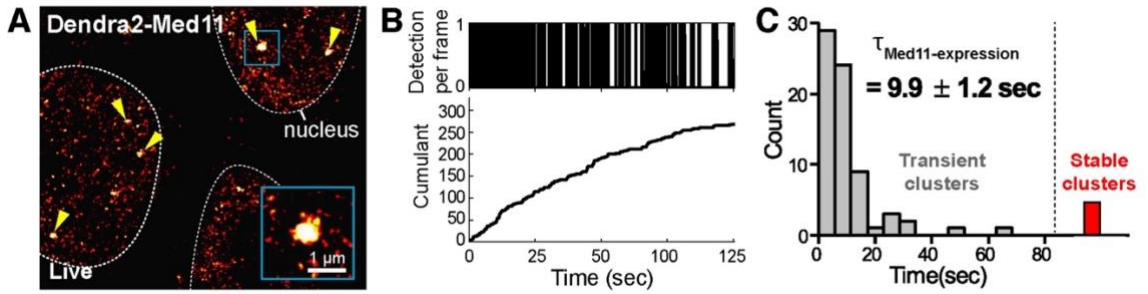

Fig. S3. Mediator clusters in Dendra2-Med11 overexpressed mESCs

Labeling of another Mediator subunit, Med11, with Dendra2 (*42, 43*). (**A**) Super-resolved image of over-expressed Dendra2-Med11 in live mESCs. Yellow arrows indicate Mediator clusters, and a blue box shows zoom-in image of one of the cluster (**B**) Corresponding tcPALM trace of the cluster highlighted in A showed a temporal detection profile of a stable cluster (**C**) Lifetime distribution of Dendra2-Med11 clusters (N=89 from 6 cells). Red bar indicates stable clusters (5.6%).

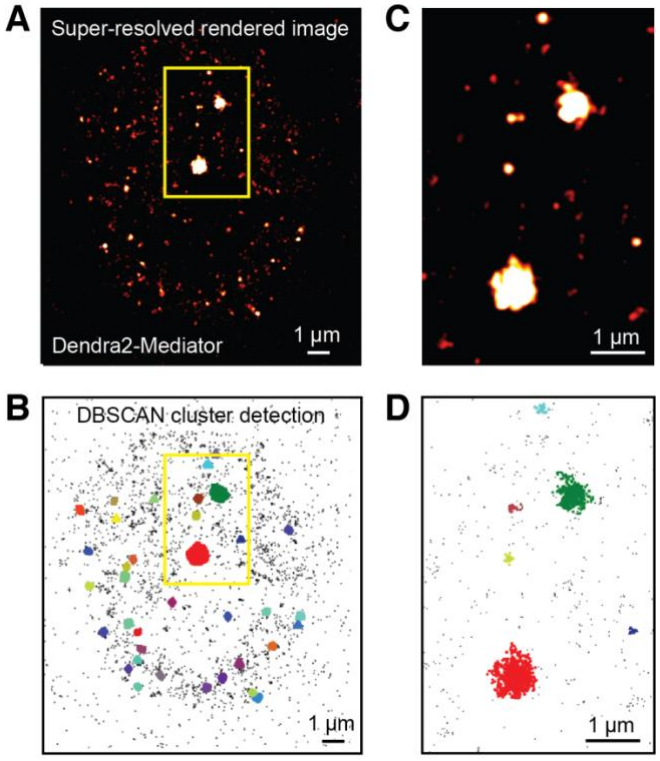

Fig. S4. DBSCAN analysis for cluster size measurement

(**A**) A super-resolved image of Dendra2-Mediator mESC. (**B**) DBSCAN analysis result for the corresponding cell in A, with parameters of N = 15 (points) and R = (100 nm). Color code represents different clusters. (**C**) A super-resolved image of a region of interest (yellow box in A). (**D**) Corresponding DBSCAN analysis result for the region of interest. Grouped localizations by DBSCAN in **D** agreed with intensified regions of super-resolved image in **C**. (see **Material and Methods**)

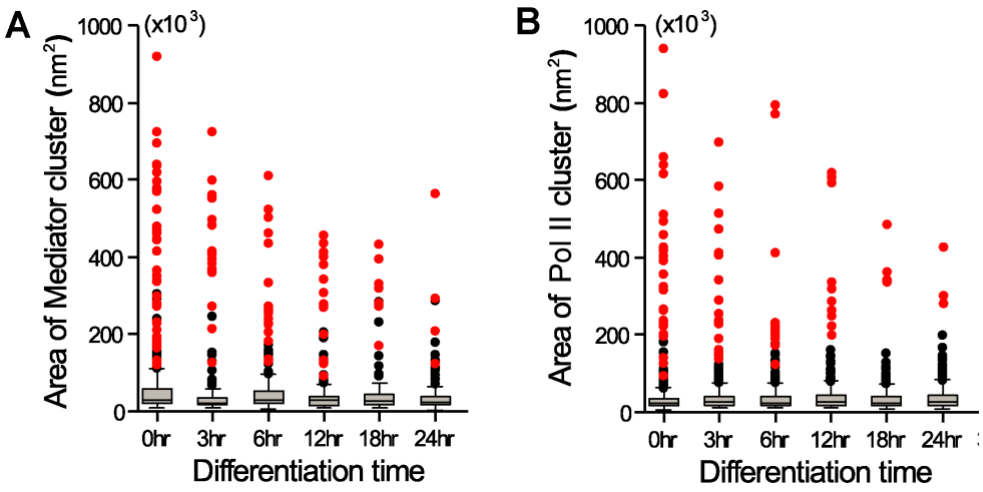

Fig. S5. Box plots of Mediator and Pol II cluster size distribution

Box plots of (**A**) Mediator and (**B**) Pol II cluster size showed that the area of clusters (red dots) as well as their number were reduced upon differentiation toward EpiLC. Clusters with stable signatures in tcPALM plots for highlighted in red (see **Fig. 1C** and **1F**).

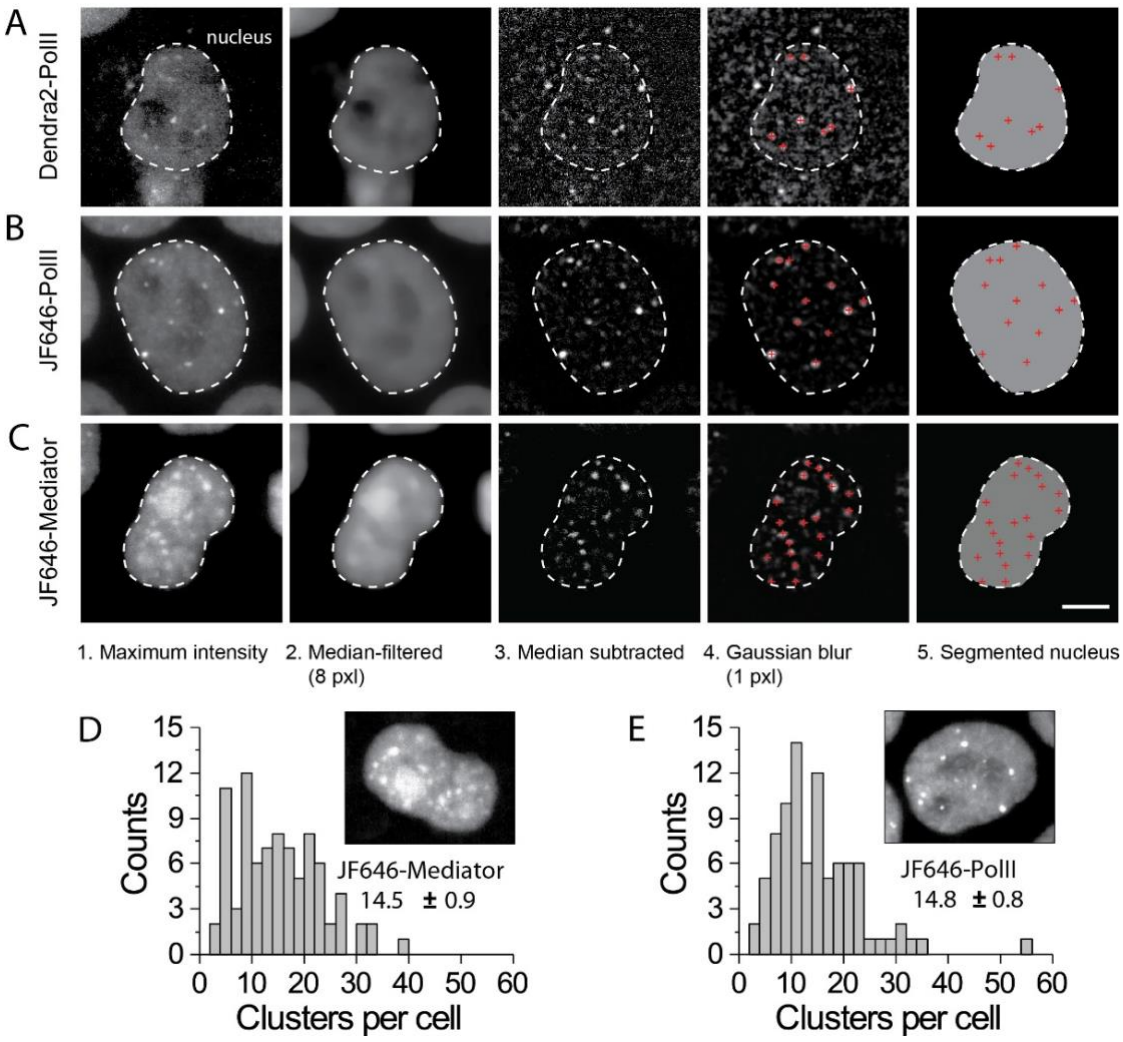

Fig. S6. Counting the number of clusters per cell nucleus

Illustration of the procedure for counting the number of stable clusters per cell using Lattice Light Sheet Microscopy. (**A**) Dendra2-Pol II. (**B**) JF646-Pol II. (**C**) JF646-Mediator. Left to right for each panel: 1. Maximum intensity projection of 3D stack. 2. Median-filtered image. 3. Raw image after background subtraction. 4. Smoothed with Gaussian kernel (1 pxl radius) for peak detection above background fluctuations (red crosses). 5. Segmented cell nuclei. Scale bar, 5μm. (**D**) The average number of clusters per nucleus in JF646-Mediator was 14.5 ± 0.9 (n=88 cells). (**E**) For JF646-Pol II, we found 14.8 ± 0.8 clusters per nucleus (n=86 cells). These results are comparable with numbers obtained from super-resolution imaging in a 2D focal plane covering 1/3 – 1/4 of the nuclear volume (**Fig. S8P and R**).

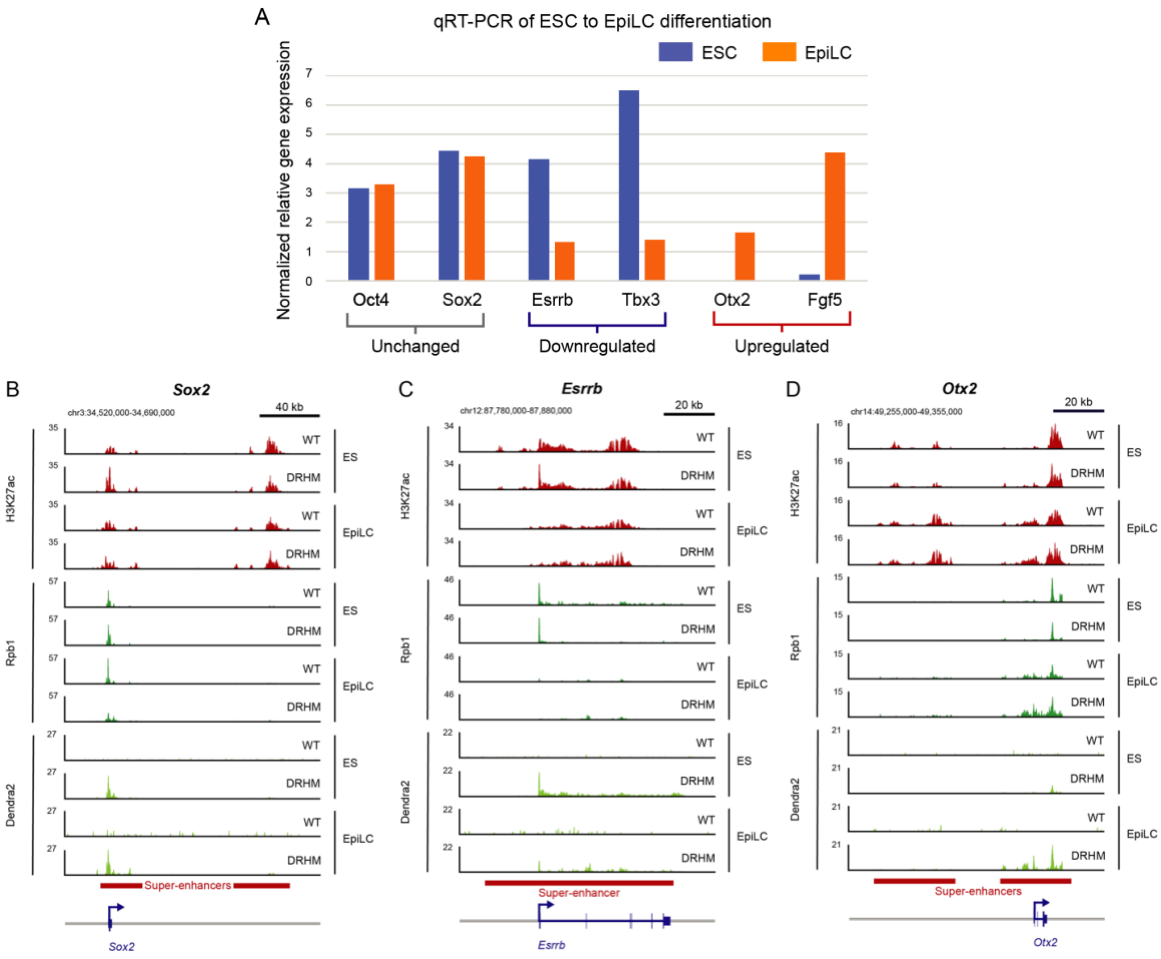

Fig. S7. qRT-PCR and Chromatin Immunoprecipitation Sequencing (Chip-seq) for CRISPR-dual-labeled Dendra2-Rpb1/Halo-Med19 (DRHM) cell line upon differentiation

Validation of stemness of the CRISPR-engineered mESC line and the EpiLC-differentiation with qPCR and Chip-sequencing. (**A**) qRT-PCR results of Oct4, Sox2, Esrrb, Tbx3, Otx2 and Fgf5 expression levels for mESCs (blue bars) and 24-hour differentiated cells (orange bars). Expected gene expression variations for the differentiation – downregulation of Esrrb, Tbx3; upregulation of Otx2, Fgf5; while expression of Oct4, Sox2 maintained– are used as validation for EpiLC differentiation (*17*). (**B**-**D**) Chip-seq panels showing H3K27ac-, Rpb1- and Dendra2-Chip-seq binding profiles of wild-type (WT) mESC and CRISPR-dual-labeled Dendra2-Rpb1/Halo-Med19 (DRHM) cell line before and after EpiLC-differentiation. (**B**) Chip-seq profiles of H3K27ac and Rpb1 for *Sox2* gene. (**C**) Chip-seq profiles of H3K27ac and RPB1 for *Esrrb* gene. (**D**) Chip-seq profiles of H3K27ac and Rpb1 for *Otx2* gene.

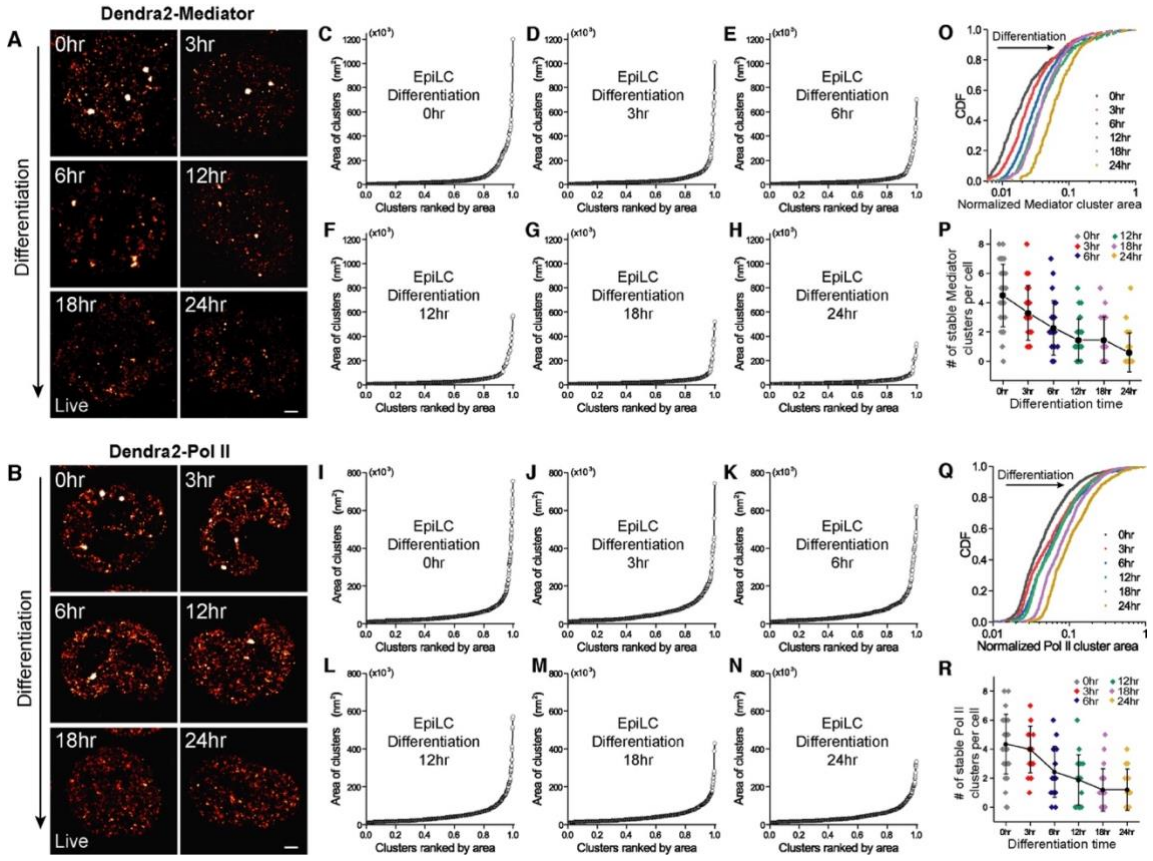

Fig. S8. Mediator and Pol II clusters gradually disappear with differentiation.

(**A, B**) Super-resolved images of Dendra2-Mediator and Dendra2-Pol II, under differentiation towards Epiblast-like cells (EpiLCs), at 0, 3, 6, 12, 18 and 24 hours after differentiation buffer exchange. Rank-ordered cluster size distributions, at 0, 3, 6, 12, 18 and 24 hours upon differentiation for (**C-H**) Mediator and (**I-N**) Pol II, respectively. Cumulative distribution function (CDF) plots of normalized cluster area distribution upon EpiLC-differentiation for (**O**) Mediator and (**Q**) Pol II, respectively. Cluster area is measured by DBSCAN Analysis (**Fig. S4**). Time-curves of number of stable clusters per cell, upon differentiation for (**P**) Mediator and (**R**) Pol II, respectively. N=21.8 ± 2.1(s.d.) cells and N=21.5 ± 4.5(s.d.) cells were analyzed at each differentiation time point (i.e. each for 0, 3, 12, 18 and 24h) for Mediator and Pol II, respectively. Scale bars represent 1 µm. All cells represented are live cells.

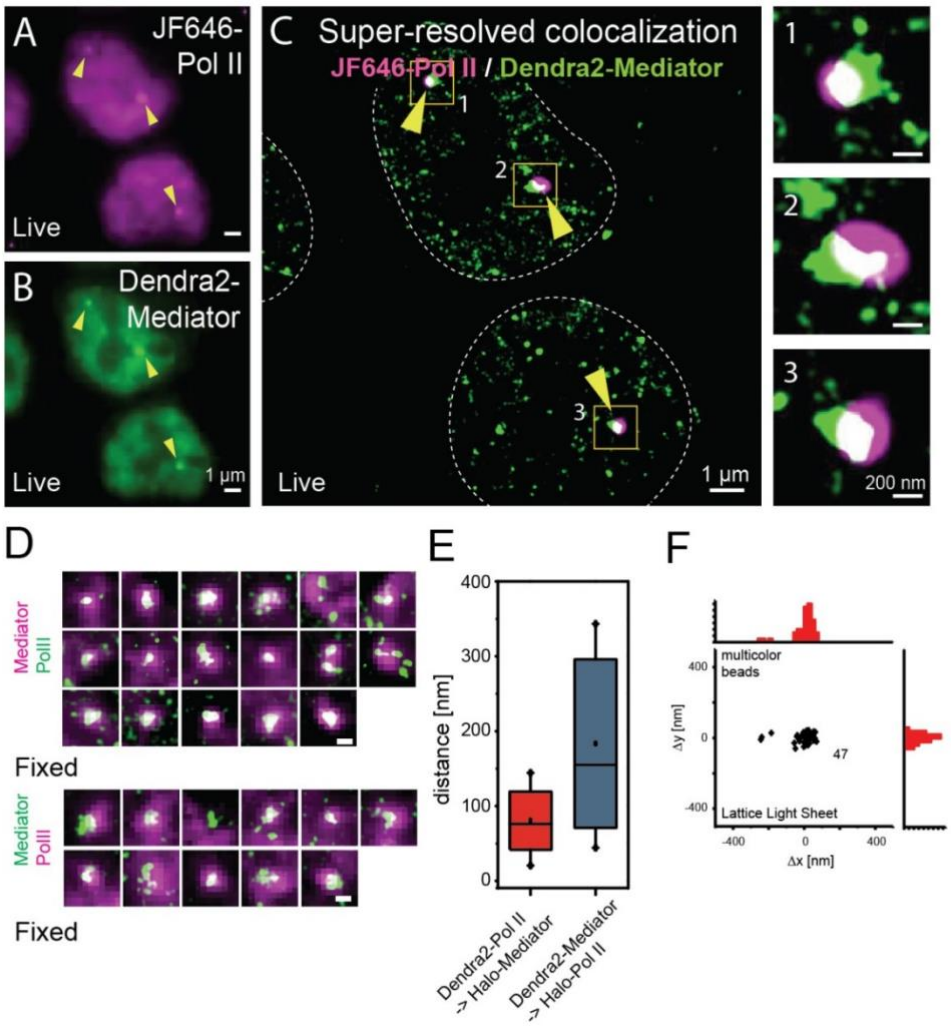

Fig. S9. Colocalization quantification

(**A**-**E**) Quantification of colocalization from 2D images. (**A** and **B**) Direct images of cells expressing both JF646-Pol II and Dendra2-Mediator. (**C**) Live cell super-resolution image of Dendra2-Mediator overlaid with a thresholded image of JF646-Pol II. Right panels show zoom-in of colocalizing clusters (yellow boxes). (**D**) Fixed cell super-resolution and epi fluorescence image overlay of clusters. (**E**) Box plot of distance distribution from super-resolved centroid to epi fluorescence centroid in ROIs shown in **C**. (**F**) Multicolor bead colocalization on the lattice light sheet microscope. Scatter plot for the distance between bead position in the 488nm channel and 642nm channel (n=47) and histograms along x and y axis.

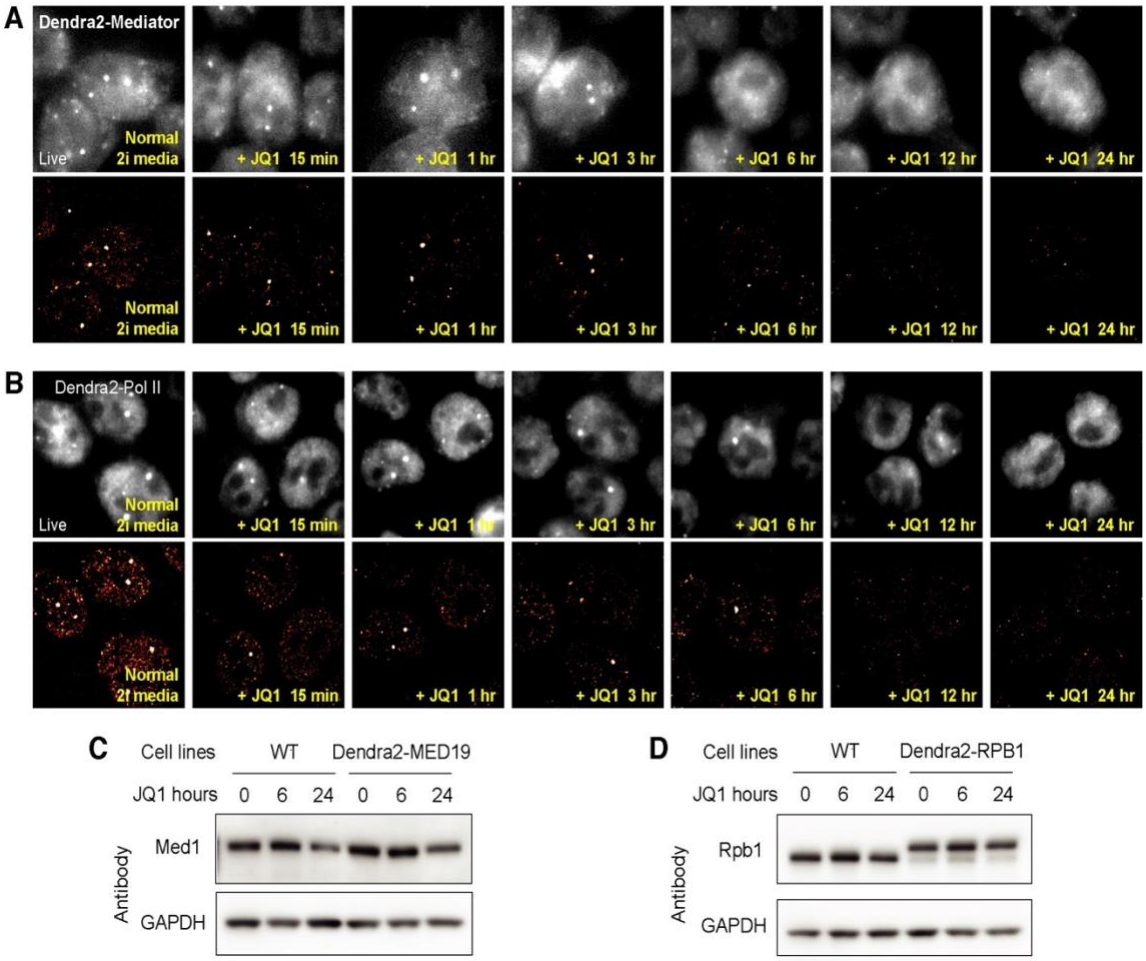

Fig. S10. Dissolution of Mediator/Pol II clusters and western-blot for JQ1 treatment

(**A,** Upper panels) Time-dependent epi-fluorescence images (488-nm excitation) of Dendra2-Mediator cells and (**A,** lower panels) time-dependent PALM super-resolution images for the corresponding cells after 1uM JQ1 treatment. (**B**, Upper panels) Time-dependent epi-fluorescence images of Dendra2-Pol II cells and (**B**, lower panels) time-dependent PALM super-resolution images for the corresponding cells after 1uM JQ1 treatment. (**C**) Western-blot of Mediator subunit, Med1, for WT mESC and CRISPR-labeled Dendra2-Med19 cell line. (**D**) Western-blot of RNA Polymerase II subunit, Rpb1, for WT mESC and CRISPR-labeled Dendra2-Med19 cell line.

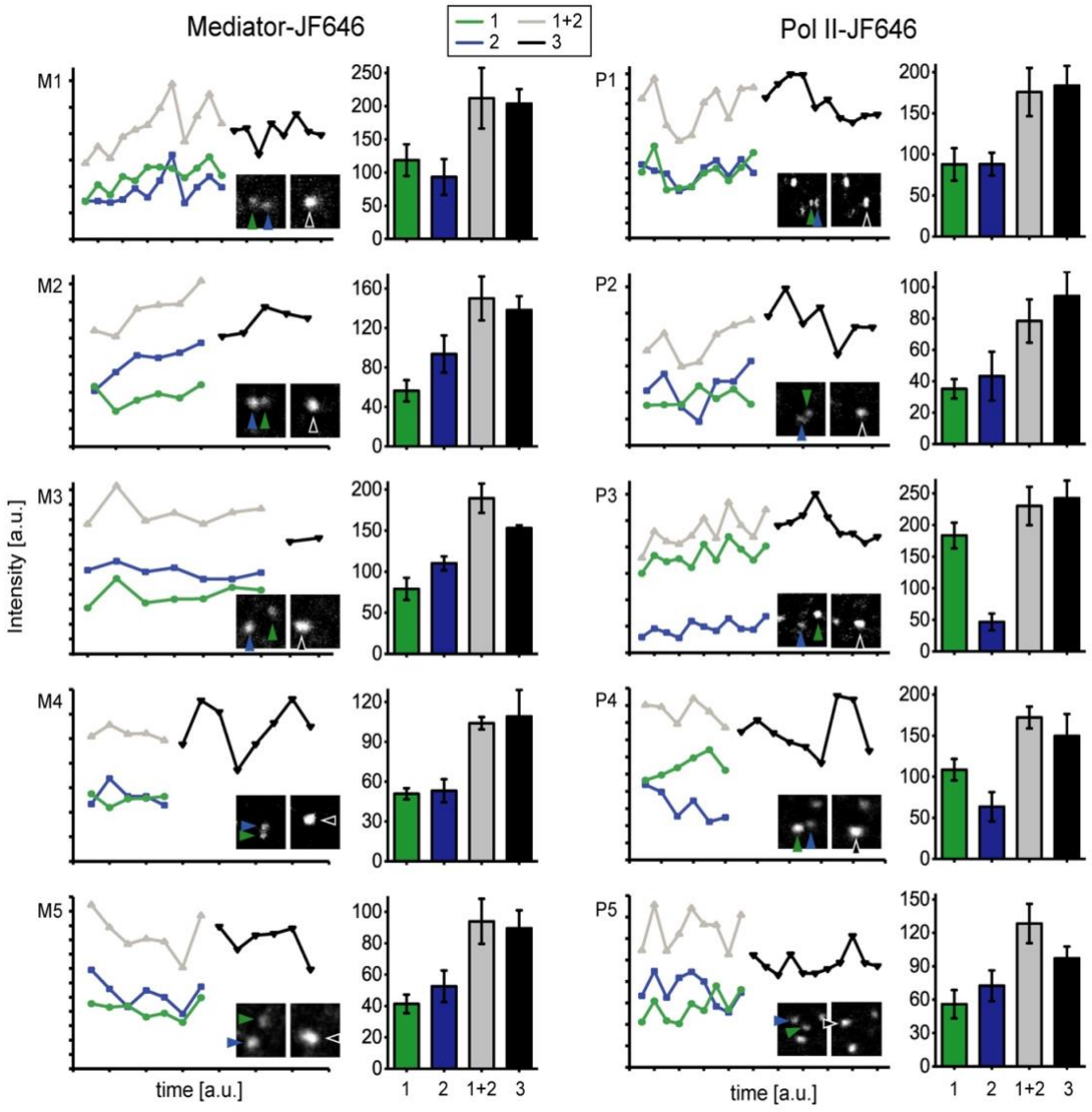

Fig. S11. Statistics of cluster fusion events

Intensity traces of clusters undergoing fusion events. Displayed are 5 fusion events for Mediator (left) and Pol II (right) each. Insets show clusters before (orange, blue) and after (black) the fusion event. Arrowheads mark clusters undergoing fusion. Bar graphs show average intensities of corresponding trajectories. Error bars represent standard deviation. With our current methods we estimated the frequency of fusion events to be about 1 event in 30-120min per cell.

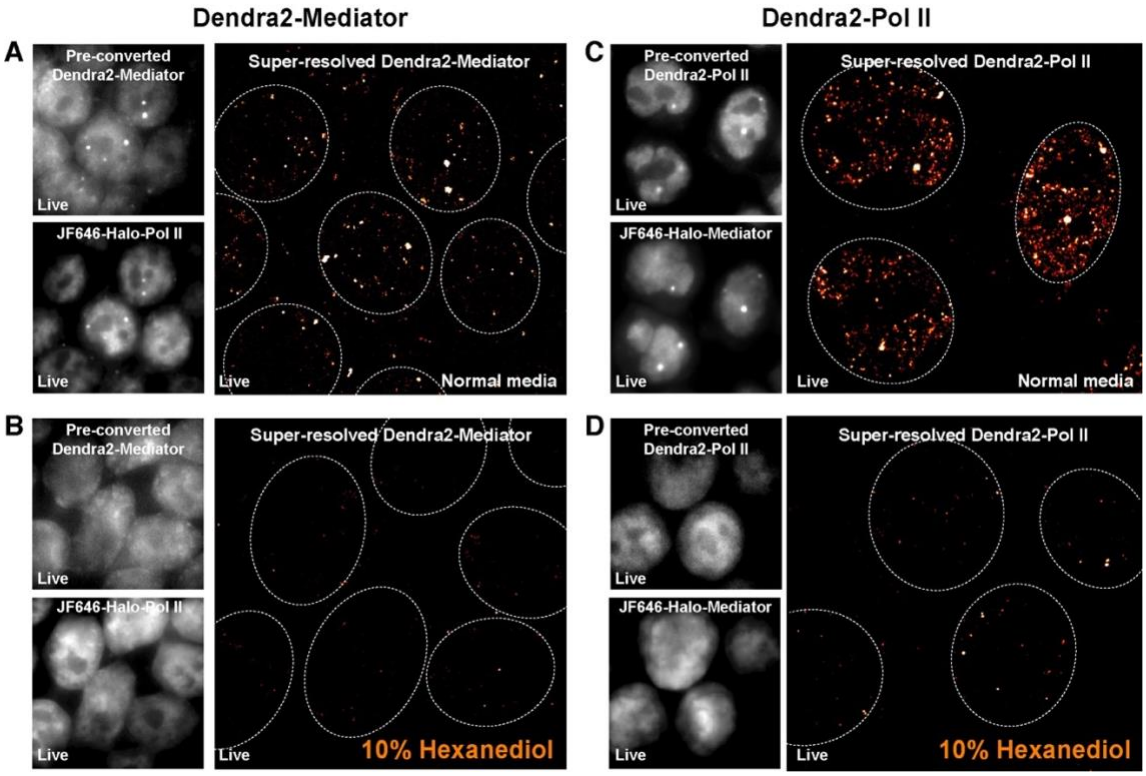

Fig. S12. Mediator and Pol II clusters dissolve with hexanediol treatment

(**A** and **B**) Dendra2-Mediator / JF646-Halo-Pol II images before and after 10% hexanediol treatment. (**C** and **D**) Dendra2-Pol II / JF646-Halo-Mediator images before and after 10% hexanediol treatment. Epi-fluorescence images (left panels).

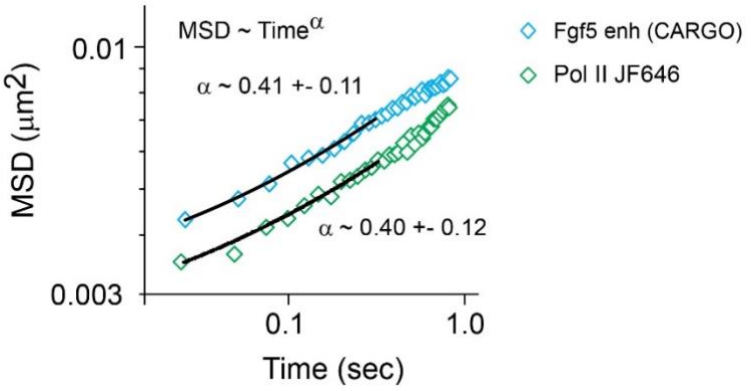

Fig. S13. Mobility of chromatin loci and clusters

Mean square displacement (MSD) of the dCas9-GFP labelled *Fgf5* enhancer locus (*23*) and Pol II-JF646 clusters. On short timescales <300ms both showed an exponent $\alpha \sim 0.4$ indicative of confined diffusion. The smaller offset of the Pol II cluster MSD as compared to the *Fgf5* enhancer locus resulted from a better signal to noise ratio.

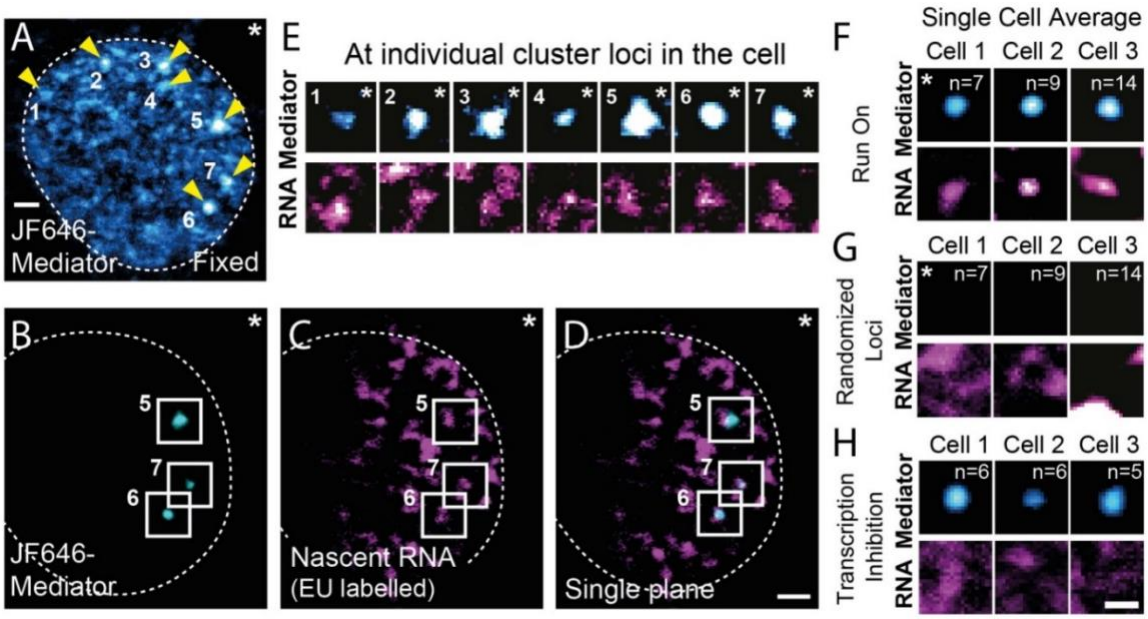

Fig. S14. Nascent RNA pulse labelling

(A) Maximum intensity projection of a fixed JF646-Mediator cell imaged using lattice light sheet microscopy. Arrowheads indicate clusters. (**B**) Single plane from a 3D stack after background subtraction showing three clusters. (**C**) Nascent RNA was labelled in the same cell using an ethynyl uridine (EU) run on assay and Click-labelling. EU was incubated for 2min before fixation. Boxes highlight the positions of clusters identified in (**B**). (**D**) Overlay of the signal revealed that accumulations of nascent RNA occured at cluster positions. (**E**) Signal from single planes centered on the JF646-Mediator clusters. RNA accumulation was detected at all clusters. (**F**) Averaged signal for all clusters in individual cells with number of clusters identified in each cell indicated. In all cases, we found accumulation of nascent RNA at clusters. (**G**) As a control for the observed RNA accumulation we randomly picked sites within the nucleus instead of the cluster positions and performed the same analysis. Only a diffuse signal was visible in the RNA channel. (**H**) When EU was incubated before DRB washout we also found only diffuse RNA signal. Scale bars 2µm (**A-D**), 1µm (**F-G**).

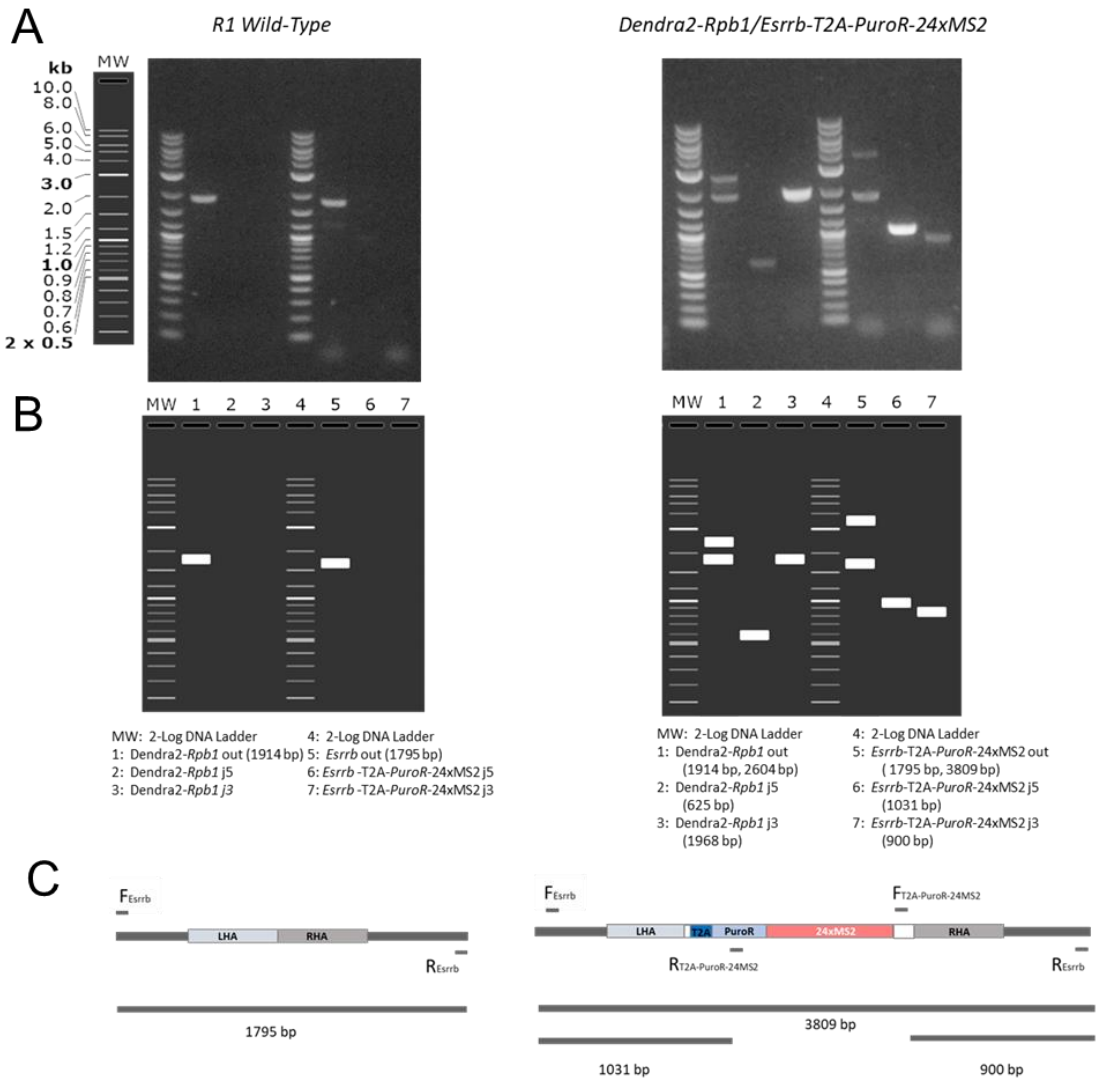

Fig. S15. MS2-insertion validation by PCR

(A) Genomic DNA was amplified by PCR from wild-type and *Esrrb*-T2A-*PuroR*-24xMS2 cell lines using primers listed in **Table S9. (B)** Expected fragments are plotted with a legend that matches lane numbers to PCR products of interest. **(C)** The PCR products for *Esrrb* sequencing are represented in context under the wild-type and modified gene locus WT-*Esrrb* (left), *Esrrb*-T2A-*PuroR*-24xMS2 (right). A partial sequence of the modified allele is reported in **Table S10.**

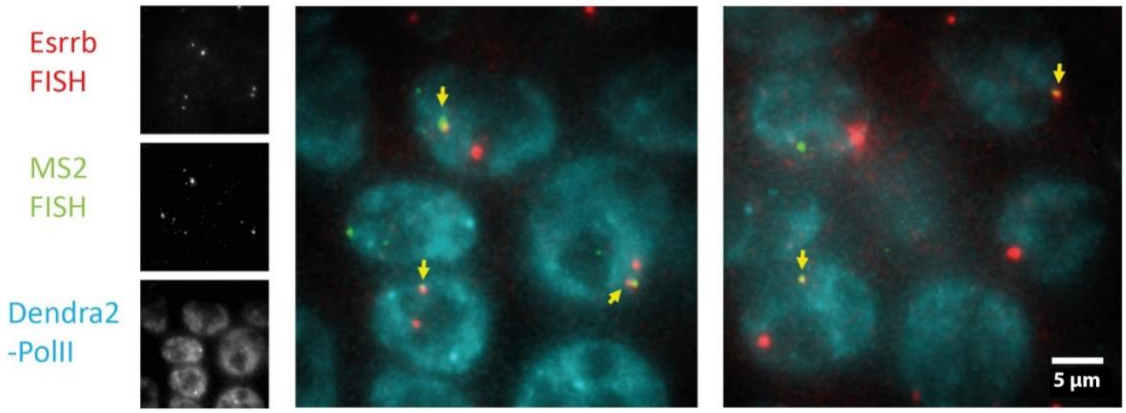

Fig. S16. Dual-color FISH for Esrrb and the MS2 sequence.

We performed dual-color FISH in fixed cells to confirm insertion of the 24xMS2 cassette in the *Esrrb* locus. Images were acquired using epi-fluorescence microscopy. Foci detected in the MS2 FISH channel colocalized with Esrrb loci. Note that only one allele of *Esrrb* contained the MS2 insertion, but both alleles were expressed as indicated by the two *Esrrb* loci detected per cell.

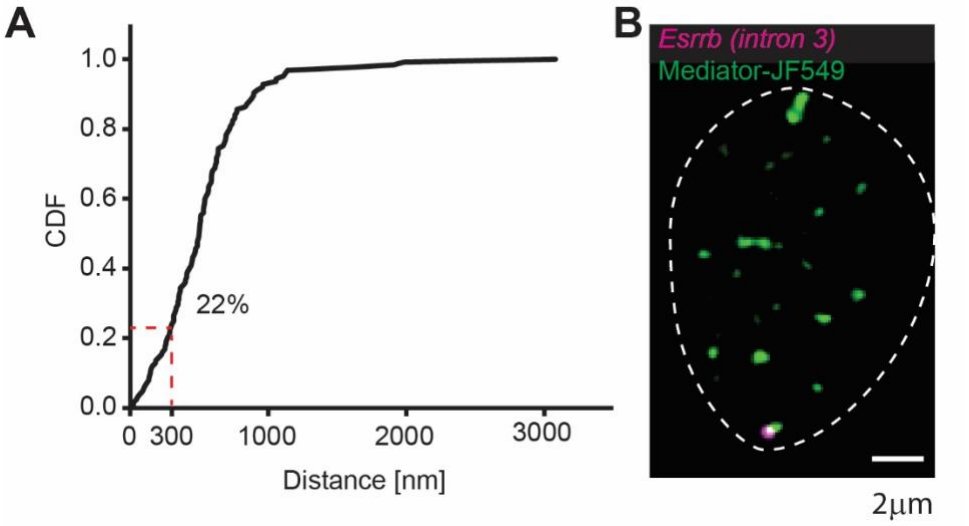

Fig. S17. Quantification of colocalization between Esrrb gene locus and clusters.

(**A**) Quantification of colocalization between the *Esrrb* locus and Mediator-JF549 by measuring the distance from Esrrb transcription sites identified by intronic FISH (intron 3) to the nearest cluster using lattice light sheet microscopy. Across 125 transcription sites identified in 82 cells we found a cluster to colocalize (<300nm, 2D distance) with 22% of the loci. We note that 93% of the loci had a cluster within a distance of 1μm. (**B**) Representative image (single plane) showing *Esrrb* locus (magenta) and Mediator-JF549 clusters.

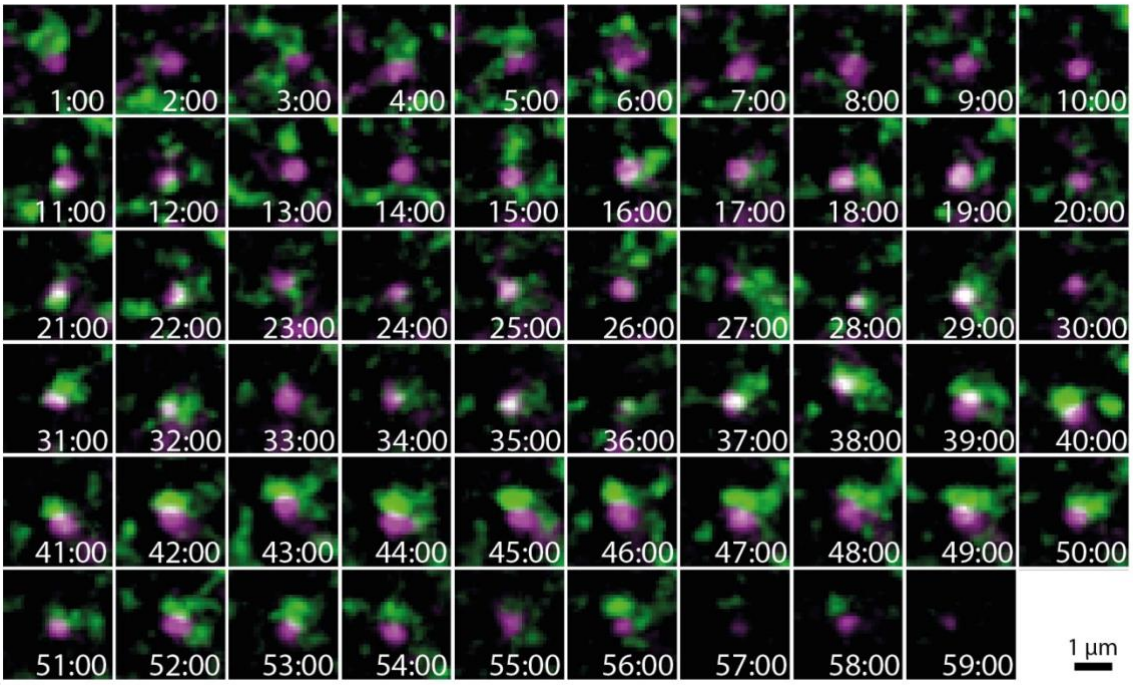

Fig. S18. Full image sequence of Esrrb-MS2 interaction with a cluster

Panels show a single plane from a 3D stack after background subtraction centered on the *Esrrb* locus. Magenta: *Esrrb*-MCP-JF646 signal. Green: Mediator-JF549 signal. Compare **Movie S3**.

Table S1. Oligo sequences for cloning sgRNAs

sgRNA	5'-3' Oligonucleotide Sequence
Med19_sgRNA #1	(forward) CACCGAAGTAATTAACGCCCGATCC
	(reverse) AAACGGATCGGGCGTTAATTACTTC
Med19_sgRNA #2	(forward) CACCGAGTAATTAACGCCCGATCCC
	(reverse) AAACGGGATCGGGCGTTAATTACTC
Med19_sgRNA #3	(forward) CACCGACGCCCGATCCCGGGTAACC
	(reverse) AAACGGTTACCCGGGATCGGGCGTC
RPB1_sgRNA # 1	(forward) CACCGCTCTCTTGATGGTGCGCAGC
	(reverse) AAACGCTGCGCACCATCAAGAGAGC
RPB1_sgRNA # 2	(forward) CACCGAGTCCTGAGTCCGGATGAAT
	(reverse) AAACATTCATCCGGACTCAGGACTC
RPB1_sgRNA # 3	(forward) CACCGCGGGGCATGCGCTGTCCCCGG
	(reverse) AAACCCGGGGACAGCGCATGCCCGC
ESRRB_sgRNA	(forward) CACCGTGCTGGAGGCCAAGGTGTGA
	(reverse) AAACTCACACCTTGGCCTCCAGCA

* Red : overhang sequences for BbsI cloning

Table S2. PCR primers for repair template amplification

Full Primer Name	5'-3' Sequence
Med19_R-T_short Fwd	CCAGACCCGGATGTAGATCTCTTATTGG
Med19_R-T_short Rev	CCGCATCAGGTAGAAGGGGC
RPB1_R-T_short Fwd	CAGCCAGTTCTCTCCTCAGAAGCG
RPB1_R-T_short Rev	CAACCCTGTCTCGTTGAACCGCAGC

Table S3. Gibson Assembly primers for Halo-*Med19*

Full Primer Name	5'-3' Sequence
Med19-Gibson-40_F	CGACGCTCGAGATTTCCGGCATGGAGAACTTCACGGCACT
Med19-Gibson-40_R	CCAGTACCGATTTCTGCCATAGCACTCTGCGCTGC
Halo-Gibson-40_F	AACCAGCAGCGCAGAGTGCTATGGCAGAAATCGGTACTGGC
Halo-Gibson-40_R	AGTGCCGTGAAGTTCTCCATGCCGGAAATCTCGAGCGT

Table S4. AarI cloning primers for Halo-*Rpb1*

Full Primer Name	5'-3' Sequence
RPB1 Halo AarI F	TCACCTGCTTTTATGCACGGGGGTGG
RPB1 Halo AarI R	TCACCTGCTTTTCCATGGCGAGGCAGGCG
Halo-RPB1 AarI F	TCACCTGCAAAAATGGCAGAAATCGGTACTGG
Halo-RPB1 AarI R	TCACCTGCTTTTGCATGCCGGAAATCTCGAGCG

Table S5. Custom fragments for EF1α-NLS-MCP-SNAP and *Esrrb* HDR plasmid cloning

Fragment Name	5'-3' sequence
AarI-gblock-v2	AAAcacctgcAAAATCAGaagtataggaacttcGgatcCGCTACTAACTTCAGCCTGCT GAAGCAGGCTGGCGACGTGGAGGAGAACCCTGGACCTAcgcgtggtcaccgagctcgaa ttcgaagttcctatactcctatAAAAgcaggtgAAA
AarI-gblock-adaptor F	AAAcacctgcACCTctataagaataggaacttcggaataggaacttcCCCAGCTGAgat ATCCGACATGTTGTTAACCCAGCCTGGGGTGCCTAATGAG
AarI-gblock-adaptor R	TTTcacctgcTTTTctgatagaataggaacttcggaataggaacttcTTgataTCGGCA GCTGTTAACCaattgTTTGCCTTCCGCCAATTCGC
T2A-PuroR-EagI_F	CCTcggccgTCCGGAGGAGAGGGCAG
T2A-PuroR-BamHI_R	ACTggatccTCACGCTCCAGGCTTCCT
SNAP-AarI-XbaI F	AAcacctgcAAAACTAGaatggacaaagactgcgaaatgaagc
SNAP-AarI-BsrGI R	AAcacctgcAAAAGTACAAacccagcccaggcttg
AarI-placeholder-oligo-F	CATGCTAGTTTTGCAGGTGAAAAGGGGTTTTCACCTGCAAAAcgcg
AarI-placeholder-oligo R	ggcccgcgTTTTGCAGGTGAAAACCCCTTTTCACCTGCAAAActag

Table S6. Plasmid Sources for EF1α-NLS-MCP-SNAP and *Esrrb* HDR plasmid cloning

Plasmid Name	**source**
16AANK7P_1841307_Actb	Geneart
pDZ415 (24MS2SL loxP-Kan-loxP)	gift from Robert Singer & Daniel Zenklusen (Addgene plasmid # 45162)
pCRISPaint-HaloTag-PuroR	gift from Veit Hornung (Addgene plasmid # 80960)
pDendra2-C	Clontech
phage ubc nls ha 2xmcp HALO	gift from Jeffrey Chao (Addgene plasmid # 64540)
pHAGE-EFS-MCP-3XBFPnls	gift from Thoru Pederson (Addgene plasmid # 75384)
pENTR4-SNAPf (w878-1)	gift from Eric Campeau (Addgene plasmid # 75384)

Table S7. PCR primers for *Rpb1* sequence validation

Full Primer Name	**5'-3' Sequence**	**Primer Symbol**	**Amplified Region**		
mmRPB1-seq F	GAGCCCTAGCGTCAACAACT	F_{out}	**WT-*Rpb1*:**	**Dendra2-*Rpb1*:**	**Halo-*Rpb1*:**
			1…1914	1…2604	1…2805
mmRPB1-seq R	CCTCTGGTATCAGCTCCCCT	R_{out}	(1914 bp)	(2604 bp)	(2805 bp)
mmRPB1 D2 j5 F	GAGCCCTAGCGTCAACAACT	F_{out}		1…625 (625 bp)	
mmRPB1 D2 j5 R	GTTCACGTTGCCCTCCATGT	$R_{Dendra2+72}$			
mmRPB1 D2 j3 F	ATTAACCTGATCAAGGAGGACAT	$F_{Dendra2+15}$		569…2536 (1968 bp)	
mmRPB1 D2 j3 R	TATTTTGTGTCGGTCTGTGAGGT	$R_{out-2536}$			
mmRPB1 HA j5 FWD	TAGGGTTTCCTTGACCCCGA	$F_{out-620}$			-620…584
mmRPB1 HA j5 REV	CGAATGGAAAGCCAGTACCGA	$R_{Halo+31}$			(1204 bp)
mmRPB1 HA j3 FWD	ATTATGTGGAAGTCCTGGGCGA	$F_{Halo+37}$			591…2103
mmRPB1 HA j3 REV	CCCATGACACTTGTTTCCTCCA	$R_{out-702}$			(1513 bp)

Table S8. PCR primers for *Med19* sequence validation

Full Primer Name	**5'-3' Sequence**	**Primer Symbol**	**Amplified Region**		
mmMed19-seq F	GACCATTGCAAATCGGTGGC	F_{out}	**WT-*Med19*:**	**Dendra2-*Med19*:**	**Halo-*Med19*:**
			1…1051	1…1741	1…1942
mmMed19-seq R	CCCGAGTTCTAAACAACGGC	R_{out}	(1051 bp)	(1741 bp)	(1942 bp)
mmMed19-D2-j5 F	GACCATTGCAAATCGGTGGC	F_{out}		1…734 (734 bp)	
mmMed19-D2-j5 R	GGATGTCGTAGCTGAAGGGC	$R_{Dendra2+184}$			
mmMed19-D2-j3 F	CCTGATCAAGGAGGACATGC	$F_{Dendra2+20}$		571…1741 (1171 bp)	
mmMed19-D2-j3 R	CCCGAGTTCTAAACAACGGC	R_{out}			
mmMed19-HA-j5 F	GACCATTGCAAATCGGTGGC	F_{out}			1…864 (864 bp)
mmMed19-HA-j5 R	TGAATGACCAGGACGACCTC	$R_{Halo+314}$			
mmMed19-HA-j3 F	ATTATGTGGAAGTCCTGGGCGA	$F_{Halo+37}$			588…1942 (1355 bp)
mmMed19-HA-j3 R	CCCGAGTTCTAAACAACGGC	R_{out}			

Table S9. PCR primers for *Esrrb*-T2A-*PuroR* sequence validation

Full Primer Name	5'-3' Sequence	Primer Symbol	WT-*Esrrb*:	*Esrrb*-MS2:
mmEsrrb j5 F	CTGTAAGCATCCCAAGCCGA	F_{Esrrb}	1…1795 (1795 bp)	1…3809 (3809 bp)
mmEsrrb j3 R	GCCCTTTAGAGCTCCTTCCTTT	R_{Esrrb}		
mmEsrrb j5 F	CTGTAAGCATCCCAAGCCGA	F_{Esrrb}		1…1031 (1031 bp)
T2A-PuroR-24xMS2 j5 R	ACGTCGTCTCTTGTAGCCAAC	$R_{T2A\text{-}PuroRo\text{-}24MS2}$		
T2A-PuroR-24xMS2 j3 F	tgcaggtcgacaaggtcac	$F_{T2A\text{-}PuroRo\text{-}24MS2}$		2708…3809 (900 bp)
mmEsrrb j3 R	GCCCTTTAGAGCTCCTTCCTTT	R_{Esrrb}		

Table S10. PCR-validated sequences

Dendra2-*Rpb1*

...CCGCGCGCGCTCCGTGTAGGCCGGTGCGGGCGGCCCCGTAGCGCAAGGGAGGGCGGGAAAGGAAGGGGCGGGACACAAGGGCGAAT
CTATAAAGGGCGTCACTCAGCCAGTTCTCTCCTCAGAAGCGCCGAGAGCGCGACCGGGACGGTTGGAGAAGAAGGTGGCTCCCGGAAGG
GGGAGAGACAAACTGCCGTAACCTCTGCCGTTCAGGATCCCGGTTACTTATTTATTCGTTACCCCTTTTcttcttcctccctcccaaaa
cctcctcctctcctcccttcttttgtttccttttttgGGAGCCGACGAATCTCCGGAAAGGGAGAAAAGGCTTTCTTTCAGCCCTTTTCG
TTCCTCTGCCTtccccccccttcccccctccccacctttccctcctccagcctttccctcccTATCCCGGGAGGTCTTTCCTGGTGG
CCGCCCGGACGGGTTCTGAGCACTTAGGCGGCGGTGGCGCAGGCTTTTTGTAGCGAGGTTTGCGCCTGCGCAGCGCGCCTGCCTCGCCA
TGAACACCCCGGGAATTAACCTGATCAAGGAGGACATGCGCGTGAAGGTGCACATGGAGGGCAACGTGAACGGCCACGCCTTCGTGATC
GAGGGCGAGGGCAAGGGCAAGCCCTACGAGGGCACCCAGACCGCCAACCTGACCGTGAAGGAGGGCGCCCCCCTGCCCTTCAGCTACGA
CATCCTGACCACCGCCGTGCACTACGGCAACCGGGTGTTCACCAAGTACCCCGAGGACATCCCCGACTACTTCAAGCAGAGCTTCCCCG
AGGGCTACAGCTGGGAGCGCACCATGACCTTCGAGGACAAGGGCATCTGCACCATCCGCAGCGACATCAGCCTGGAGGGCGACTGCTTC
TTCCAGAACGTGCGCTTCAAGGGCACCAACTTCCCCCCCAACGGCCCCGTGATGCAGAAGAAGACCCTGAAGTGGGAGCCCAGCACCGA
GAAGCTGCACGTGCGCGACGGCCTGCTGGTGGGCAACATCAACATGGCCCTGCTGCTGGAGGGCGGCGGCCACTACCTGTGCGACTTCA
AGACCACCTACAAGGCCAAGAAGGTGGTGCAGCTGCCCGACGCCCACTTCGTGGACCACCGCATCGAGATCCTGGGCAACGACAGCGAC
TACAACAAGGTGAAGCTGTACGAGCACGCCGTGGCCCGCTACAGCCCCCTGCCCAGCCAGGTGTGGATGCACGGGGGTGGCCCCCCCTC
CGGCGACAGCGCATGCCCGCTCCGCACCATCAAGAGAGTGCAGTTCGGAGTCCTGAGCCCGGATGAATTGGTAAGATAGTCCGCCCGTC
TCTCTGCTATGCCTTTGGCTGATGATCCTCTGGGAAGATGGGTCAGTGATGCTGATGTTGTGCGGGGGTCCAGCCTTCAAAAGTTAAAT
TATGCCAGGACTTAAACAAGCGAAATGCTATGCCTGAGATGAGTGCTTGACTGGACAGAGAAGAAAGATGTTTCCATACTTGAGCATTG
CTGCGGTTCAACGAGACAGGGTTGAAAGTTGTACAGGAAGTGGATCCCCAGTTTTAGTTCTTTCACCAATATTGAGCATCCTGCTATGT
GACAGTAATCAGACACTAGGAACACAGCTGCACAATAAATATAACAGAAACTCTACCTTCTAAAACACTATGGGAAAAACAGAGAAGAG
AGCTTAAGAACAAAAAGAAATGAGCAAAAATAAGTACCTAGATTAAAGCAAAATGAGGAAATGCTGTAAGAAGTCACTGAAATTGAATG
GTGTCAGGGTTTGGAAGACATACTTGCCAGGGATGGTGACATTCCCAAGTAATATCAGTCATCAGAGCTATTTTTTTAGGTGGAGGAAA
CAAGTGTCATGGGACTGAGAGGGAAATAAACTTGTATTCTAGAGACTGAAAAGCCAGTGTTGGGGCAGGCAGGGTTAGTGGGTGCGGAG
AGTGCACTGAAGAAGCACGGGATATTGTAAATTACGCT...

Dendra2 start codon *RPB1* start codon silent mutations repair template

HaloTag-*Rpb1*

...GTGCGGGCGGCCCCGTAGCGCAAGGGAGGGCGGGAAAGGAAGGGGCGGGACACAAGGGCGAATCTATAAAGGGCGTCACTCAGCCA
GTTCTCTCCTCAGAAGCGCCGAGAGCGCGACCGGGACGGTTGGAGAAGAAGGTGGCTCCCGGAAGGGGGAGAGACAAACTGCCGTAACC
TCTGCCGTTCAGGATCCCGGTTACTTATTTATTCGTTACCCCTTTTCTTCTTCCTCCCTCCCAAAACCTCCTCCTCTCCTCCCTTCTTT
TGTTTCCTTTTTGGGAGCCGACGAATCTCCGGAAAGGGAGAAAAGGCTTTCTTTCAGCCCTTTTCGTTCCTCTGCCTTCCCCCCCCCTT
CCCCCCTCCCCCACCTTTCCCTCCTCCAGCCTTTCCCTCCCTATCCCGGGAGGTCTTTCCTGGTGGCCGCCCGGACGGGTTCTGAGCAC
TTAGGCGGCGGTGGCGCAGGCTTTTTGTAGCGAGGTTTGCGCCTGCGCAGCGCGCCTGCCTCGCCATGGCAGAAATCGGTACTGGCTTT
CCATTCGACCCCCATTATGTGGAAGTCCTGGGCGAGCGCATGCACTACGTCGATGTTGGTCCGCGCGATGGCACCCCTGTGCTGTTCCT
GCACGGTAACCCGACCTCCTCCTACGTGTGGCGCAACATCATCCCGCATGTTGCACCGACCCATCGCTGCATTGCTCCAGACCTGATCG
GTATGGGCAAATCCGACAAACCAGACCTGGGTTATTTCTTCGACGACCACGTCCGCTTCATGGATGCCTTCATCGAAGCCCTGGGTCTG
GAAGAGGTCGTCCTGGTCATTCACGACTGGGGCTCCGCTCTGGGTTTCCACTGGGCCAAGCGCAATCCAGAGCGCGTCAAAGGTATTGC
ATTTATGGAGTTCATCCGCCCTATCCCGACCTGGGACGAATGGCCAGAATTTGCCCGCGAGACCTTCCAGGCCTTCCGCACCACCGACG
TCGGCCGCAAGCTGATCATCGATCAGAACGTTTTTATCGAGGGTACGCTGCCGATGGGTGTCGTCCGCCCGCTGACTGAAGTCGAGATG
GACCATTACCGCGAGCCGTTCCTGAATCCTGTTGACCGCGAGCCACTGTGGCGCTTCCCAAACGAGCTGCCAATCGCCGGTGAGCCAGC
GAACATCGTCGCGCTGGTCGAAGAATACATGGACTGGCTGCACCAGTCCCCTGTCCCGAAGCTGCTGTTCTGGGGCACCCCAGGCGTTC
TGATCCCACCGGCCGAAGCCGCTCGCCTGGCCAAAAGCCTGCCTAACTGCAAGGCTGTGGACATCGGCCCGGGTCTGAATCTGCTGCAA
GAAGACAACCCGGACCTGATCGGCAGCGAGATCGCGCGCTGGCTGTCGACGCTCGAGATTTCCGGCATGCACGGGGGTGGCCCCCCCTC
CGGCGACAGCGCATGCCCGCTCCGCACCATCAAGAGAGTGCAGTTCGGAGTCCTGAGCCCGGATGAATTGGTAAGATAGTCCGCCCGTC
TCTCTGCTATGCCTTTGGCTGATGATCCTCTGGGAAGATGGGTCAGTGATGCTGATGTTGTGCGGGGGTCCAGCCTTTCAAAAGTTAAA
TTATGCCAGGACTTAAACAAGCGAAATGCTATGCCTGAGATGAGTGCTTGACTGGACAGAGAAGAAAGATGTTTCCATACTTGAGCATT
GCTGCGGTTCAACGAGACAGGGTTGAAAGTTGTACAGGAAGTGGATCCCCAGTTTTAGTTCTTTCACCAATATTGAGCATCCTGCTATG
TGACAGTAATCAGACACTAGGAACACAGCTGCACAATAAATATAACAGAAACTCTACCTTCTAAAACACTATGGGAAAAACAGAGAAGA
GAGCTTAAGAACAAAAAGAAATGAGCAAAAATAAGTACCTAGATTAAAGCAAAATGAGGAAATGCTGTAAGAAGTCACTGAAATTGAAT
GGTGTCAGGGTTTGGAAGACATACTTGCCAGGGATGGTGACATTCCCAAGTAATATCA...

Halo start codon *RPB1* start codon silent mutations repair template

Dendra2-*Med19*

...ATCGGTGGCAGTTTCCTCACGAGGAGGAAAGCAATGGAAAGCAGAGCAGACAGAAGGCAATAAGGTCGGGCCAGCCATCGA
GAAAGCCGCGGCACCGAGTACACCAAAGCAATCAGAGGCGCAAGGACAGCCATCTTTCCTGCCTACTCTCTCGCAGGCTCACTCCCGCTCCC
CAAATCTTCGTCCTCCGCCCCCACCAGCAAGGCTTCTATTGGACCAAATATCAGATGCAACGCCTCCAGACCCGGATGTAGATCTCTTATTG
GATGCTATAATAGATCAGAAAATGAATTAAATAGTCTATTGGTCCTCATCGTTGTCGCTTTTCTAACTGAGTCATTTTATTGGCTATTAGTC
TGCGAACCACCTTCCTAACCAGTCTCTCAGGCGACGGAAGTAAGTTGCCGGAAGATGGTAGGCGGGGCTTAATGTATCCAATGATGGGACAC
TCTTAGACGAAGAGGGTGGTACCCTGTGAAAGTACTGTCCAATCAAAGTAATTAACCCCGGATCCCGCGTAACCAGCAGCGCAGAGTGCTAT
GAACACCCCGGGAATTAACCTGATCAAGGAGGACATGCGCGTGAAGGTGCACATGGAGGGCAACGTGAACGGCCACGCCTTCGTGATCGAGG
GCGAGGGCAAGGGCAAGCCCTACGAGGGCACCCAGACCGCCAACCTGACCGTGAAGGAGGGCGCCCCCCTGCCCTTCAGCTACGACATCCTG
ACCACCGCCGTGCACTACGGCAACCGGGTGTTCACCAAGTACCCCGAGGACATCCCCGACTACTTCAAGCAGAGCTTCCCCGAGGGCTACAG
CTGGGAGCGCACCATGACCTTCGAGGACAAGGGCATCTGCACCATCCGCAGCGACATCAGCCTGGAGGGCGACTGCTTCTTCCAGAACGTGC
GCTTCAAGGGCACCAACTTCCCCCCCAACGGCCCCGTGATGCAGAAGAAGACCCTGAAGTGGGAGCCCAGCACCGAGAAGCTGCACGTGCGC
GACGGCCTGCTGGTGGGCAACATCAACATGGCCCTGCTGCTGGAGGGCGGCGGCCACTACCTGTGCGACTTCAAGACCACCTACAAGGCCAA
GAAGGTGGTGCAGCTGCCCGACGCCCACTTCGTGGACCACCGCATCGAGATCCTGGGCAACGACAGCGACTACAACAAGGTGAAGCTGTACG
AGCACGCCGTGGCCCGCTACAGCCCCCTGCCCAGCCAGGTGTGGATGGAGAACTTCACGGCACTGTTTGGAGCTCAGACTGACCCCCCACCG
CCACCAAGCGCCCTAGGCTTTGGGCCTGGAAAGCCACCCCCGCCACCCCCTCCTCCTCCGGGAGGTGGTCCAGGCGCAGCCCCGCCCTCGAC
GGCAACCTCGGCCCCCGCAGGAGCGGATAAGTCGACGGCTGGAAGTGGCCCCTTCTACCTGATGCGGGAATTGCCAGGTGAGTAGTAGGCCA
AGAGTAGCCACTCAGATTGTAGTTCAGGTGAGGGTGTGGCTAGCCTGTCCCGCTAGGTGTGAGATAACAGGGCTACGCGGGGCCAGTGGGCA
ACAGTGTCAGAAGCCCTTTGGCGATTCACAACCCTAAGGGATAACTTGATTTTCTGGGGTGGGTTTGGGTTGGGTGTGAATATCTGGGACAA
CCTTCAGCGAGAAGTTCTGTGATCCGGGTTCTCTGACTGCCG...

Dendra2 start codon *Med19* start codon silent mutations repair template

HaloTag-*Med19*

...ATCGGTGGCAGTTTCCTCACGAGGAGGAAAGCAATGGAAAGCAGAGCAGACAGAAGGCAATAAGGTCGGGCCAGCCATCGA
GAAAGCCGCGGCACCGAGTACACCAAAGCAATCAGAGGCGCAAGGACAGCCATCTTTCCTGCCTACTCTCTCGCAGGCTCACTCCCGCTCCC
CAAATCTTCGTCCTCCGCCCCCACCAGCAAGGCTTCTATTGGACCAAATATCAGATGCAACGCCTCCAGACCCGGATGTAGATCTCTTATTG
GATGCTATAATAGATCAGAAAATGAATTAAATAGTCTATTGGTCCTCATCGTTGTCGCTTTTCTAACTGAGTCATTTTATTGGCTATTAGTC
TGCGAACCACCTTCCTAACCAGTCTCTCAGGCGACGGAAGTAAGTTGCCGGAAGATGGTAGGCGGGGCTTAATGTATCCAATGATGGGACAC
TCTTAGACGAAGAGGGTGGTACCCTGTGAAAGTACTGTCCAATCAAAGTAATTAACCCCGGATCCCGCGTAACCAGCAGCGCAGAGTGCTAT
GGCAGAAATCGGTACTGGCTTTCCATTCGACCCCCATTATGTGGAAGTCCTGGGCGAGCGCATGCACTACGTCGATGTTGGTCCGCGCGATG
GCACCCCTGTGCTGTTCCTGCACGGTAACCCGACCTCCTCCTACGTGTGGCGCAACATCATCCCGCATGTTGCACCGACCCATCGCTGCATT
GCTCCAGACCTGATCGGTATGGGCAAATCCGACAAACCAGACCTGGGTTATTTCTTCGACGACCACGTCCGCTTCATGGATGCCTTCATCGA
AGCCCTGGGTCTGGAAGAGGTCGTCCTGGTCATTCACGACTGGGGCTCCGCTCTGGGTTTCCACTGGGCCAAGCGCAATCCAGAGCGCGTCA
AAGGTATTGCATTTATGGAGTTCATCCGCCCTATCCCGACCTGGGACGAATGGCCAGAATTTGCCCGCGAGACCTTCCAGGCCTTCCGCACC
ACCGACGTCGGCCGCAAGCTGATCATCGATCAGAACGTTTTTATCGAGGGTACGCTGCCGATGGGTGTCGTCCGCCCGCTGACTGAAGTCGA
GATGGACCATTACCGCGAGCCGTTCCTGAATCCTGTTGACCGCGAGCCACTGTGGCGCTTCCCAAACGAGCTGCCAATCGCCGGTGAGCCAG
CGAACATCGTCGCGCTGGTCGAAGAATACATGGACTGGCTGCACCAGTCCCCTGTCCCGAAGCTGCTGTTCTGGGGCACCCCAGGCGTTCTG
ATCCCACCGGCCGAAGCCGCTCGCCTGGCCAAAAGCCTGCCTAACTGCAAGGCTGTGGACATCGGCCCGGGTCTGAATCTGCTGCAAGAAGA
CAACCCGGACCTGATCGGCAGCGAGATCGCGCGCTGGCTGTCGACGCTCGAGATTTCCGGCATGGAGAACTTCACGGCACTGTTTGGAGCTC
AGACTGACCCCCCACCGCCACCAAGCGCCCTAGGCTTTGGGCCTGGAAAGCCACCCCCGCCACCCCCTCCTCCTCCGGGAGGTGGTCCAGGC
GCAGCCCCGCCCTCGACGGCAACCTCGGCCCCCGCAGGAGCGGATAAGTCGACGGCTGGAAGTGGCCCCTTCTACCTGATGCGGGAATTGCC
AGGTGAGTAGTAGGCCAAGAGTAGCCACTCAGATTGTAGTTCAGGTGAGGGTGTGGCTAGCCTGTCCCGCTAGGTGTGAGATAACAGGGCTA
CGCGGGGCCAGTGGGCAACAGTGTCAGAAGCCCTTTGGCGATTCACAACCCTAAGGGATAACTTGATTTTCTGGGGTGGGTTTGGGTTGGGT
GTGAATATCTGGGACAACCTTCAGCGAGAAGTTCTGTGATCCGGG...

Halo start codon *Med19* start codon silent mutations repair template

***Esrrb*-T2A-*PuroR*-24xMS2**
...ATATCCCCGCCGGCTCCCTCTATCAGCACACCCTCCCCTCGCCCCCAAACACCTAGACATTGACTTCCATCCCTTTATATCTGTTCTGAG TTGTAAGGTTGGTGGCTGTACTGCATGTGAGTGGTACCCATGGCCCAGCATCATCATGAAGACGTGATGATGTCAGGGTTAGGTGATAGC CGTGAGGTTCCTAAGACCCAGGTGCTTAATTGTTGCTGTATAACTGTATGAGGTAGGTATGGCTAGGAAAATGGGGGACAGAGAAGTTA TATAATGTCTCACATAACCCAAAAGGGACTGCCAGCCAGATTCCAGAGTCCCCCGAACGCCTCTGAGACATCCAATAGGTCTGCCCATGTT CATCGGCAGTGCCCTCCTGGTGGTCTCTCTATGAGGTCTGAGCTCAGTTCTACCCTCCTCAGTCTCTGACTCAGCCCTGCATCAAAGATCCT CATTCTACTCTGAATAGTCAGTCAGCAGACAGACAGACAGAGACAGGCTGGCTGCTGGTCTGTCCTCCACTCCAGAAATGCCTTCCGTGTT GGGGGGTGGCAGCCAGCCCCTGCTGACACTGCCCCTCTCCTGTGTCCACAGATTCGATGTACATTGAGAACCTGGAGGCGGTGCAGAAG CTCCAGGACCTGCTGCACGAGGCGCTGCAGGACTATGAGCTGAGTCAGCGCCACGAGGAGCCGCGGAGGGCCGGCAAGCTGCTGCTGA CGCTGCCCCTGCTGAGGCAGACAGCCGCCAAAGCCGTGCAACACTTCTACAGCGTGAAACTGCAGGGCAAGGTGCCCATGCACAAACTCT TCCTGGAGATGCTGGAGGCCAAGGTGtggccgTCCGGAGGAGAGGGCAGAGGAAGTCTGCTAACATGCGGTGACGTCGAGGAGAATCC TGGCCCAATGACTGAATACAAGCCTACTG...24xMS2...caaggtcaccTGATGGCCCAGCACATGGACGGACGGACACGATCCAAGTGGAGA CCTCCACAGCCACCAGCCTCGACTTTTTTCACACCCGCATCGGGGCTCTGAGCTGTCCCAGAAGAAGGGGTCTTCTTGCTTCCTGGCCATGT GCAGACTCCTGGGGACAGCAGATGGGGAGGTGGGGATGGGGAGGGTAGGGGCGGGGGGCTCATCTGTCACCCGCATTTTCTTTGGAAT TTTTTTTTCCTTCTCCATGGGCAGTGCTAAGGCTTGGGCCAGGGACGACTTCCCTTAGAGCTGGAGACCACCAGAGGAAGCAGCCTTCCT GCAAGGGATCCATTTCTGGACCTCTCCCTATTTAGGACCTGGAGGTATCTGGATGGGCAGTGCTTAGTGCCCGGGACCCAAGAGACATAG ATTGGGGGCTCCTGAAGGTGTTGGTGTCACGGTGGGCAGTCCCTTGGGGCAGAACGTCTCTGTGGCCTATCCCGAGGCTCTGTTCCTCCT CCATCTAGCTGGCTCCCTCCACTTTCCCCTTTCTTATTGTCCCAGTACACCCAGTTCTCAGTGGATGCTCCTGCTAGAGTAGCCACATCCCCA CCCCGAAGAACCCCTCCCCTGCTTCCTGCCCCTACCTCAGCCAGCCGGAACTCACTGGCTCAGAAAAGAGTTGGGTTCTGTACCCACTGCT CTTTTTGCCTGCTGTTTCTCCTTCTCCTCTTGGGCATGGCCAGTCTAGAAACCTATGGAGAATTCAGGACCTGGCCCCACCAGAGGTCACTT GAGGGACTCTCAAGGTCAGTAGCTTAGGTTGGGGTGTAGGATAGCAGAGAG...
T2A *PuroR* (partial sequence) repetitive region (not sequenced) repair template

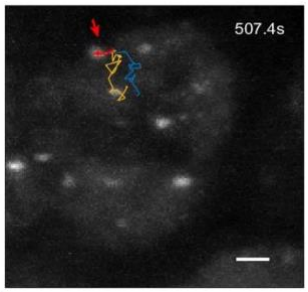

Movie S1. Pol II clusters coalescing

Typical example of Pol II clusters coalescing as discussed in **Fig. 3**. Maximum intensity projection of full cell nucleus, no background subtracted. Time is indicated in upper right corner. Scale bar 5µm.

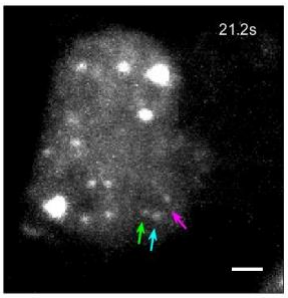

Movie S2. Mediator clusters coalescing

Typical example of Mediator clusters coalescing. Maximum intensity projection of full cell nucleus, no background subtracted. Time is indicated in upper right corner. Scale bar 1µm. Two consecutive coalescence events were observed for JF646-Mediator.

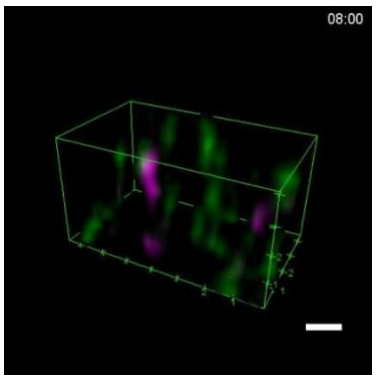

Movie S3. *Esrrb* locus and Mediator cluster 3D tracking

3D rendering of dual color lattice light sheet data showing an *Esrrb* gene locus labelled by MS2-tagged nascent mRNA dynamically interacting with a Mediator cluster. Scale bar 1 µm.

References and Notes

1. P. J. Robinson, M. J. Trnka, D. A. Bushnell, R. E. Davis, P. J. Mattei, A. L. Burlingame, R. D. Kornberg, Structure of a complete mediator-RNA polymerase II pre-initiation complex. *Cell* **166**, 1411–1422.e16 (2016). doi:10.1016/j.cell.2016.08.050 Medline

2. R. D. Kornberg, Mediator and the mechanism of transcriptional activation. *Trends Biochem. Sci.* **30**, 235–239 (2005). doi:10.1016/j.tibs.2005.03.011 Medline

3. C. T. Ong, V. G. Corces, Enhancer function: New insights into the regulation of tissue-specific gene expression. *Nat. Rev. Genet.* **12**, 283–293 (2011). doi:10.1038/nrg2957 Medline

4. K. M. Lelli, M. Slattery, R. S. Mann, Disentangling the many layers of eukaryotic transcriptional regulation. *Annu. Rev. Genet.* **46**, 43–68 (2012). doi:10.1146/annurev-genet-110711-155437 Medline

5. B. L. Allen, D. J. Taatjes, The Mediator complex: A central integrator of transcription. *Nat. Rev. Mol. Cell Biol.* **16**, 155–166 (2015). doi:10.1038/nrm3951 Medline

6. M. Levine, C. Cattoglio, R. Tjian, Looping back to leap forward: Transcription enters a new era. *Cell* **157**, 13–25 (2014). doi:10.1016/j.cell.2014.02.009 Medline

7. S. T. Hess, T. P. Girirajan, M. D. Mason, Ultra-high resolution imaging by fluorescence photoactivation localization microscopy. *Biophys. J.* **91**, 4258–4272 (2006). doi:10.1529/biophysj.106.091116 Medline

8. M. J. Rust, M. Bates, X. Zhuang, Sub-diffraction-limit imaging by stochastic optical reconstruction microscopy (STORM). *Nat. Methods* **3**, 793–796 (2006). doi:10.1038/nmeth929 Medline

9. E. Betzig, G. H. Patterson, R. Sougrat, O. W. Lindwasser, S. Olenych, J. S. Bonifacino, M. W. Davidson, J. Lippincott-Schwartz, H. F. Hess, Imaging intracellular fluorescent proteins at nanometer resolution. *Science* **313**, 1642–1645 (2006). doi:10.1126/science.1127344 Medline

10. B. C. Chen, W. R. Legant, K. Wang, L. Shao, D. E. Milkie, M. W. Davidson, C. Janetopoulos, X. S. Wu, J. A. Hammer 3rd, Z. Liu, B. P. English, Y. Mimori-Kiyosue, D. P. Romero, A. T. Ritter, J. Lippincott-Schwartz, L. Fritz-Laylin, R. D. Mullins, D. M. Mitchell, J. N. Bembenek, A. C. Reymann, R. Böhme, S. W. Grill, J. T. Wang, G. Seydoux, U. S. Tulu, D. P. Kiehart, E. Betzig, Lattice light-sheet microscopy: Imaging molecules to embryos at high spatiotemporal resolution. *Science* **346**, 1257998 (2014). doi:10.1126/science.1257998 Medline

11. D. Hnisz, K. Shrinivas, R. A. Young, A. K. Chakraborty, P. A. Sharp, A phase separation model for transcriptional control. *Cell* **169**, 13–23 (2017). doi:10.1016/j.cell.2017.02.007 Medline

12. T. Fukaya, B. Lim, M. Levine, Enhancer control of transcriptional bursting. *Cell* **166**, 358–368 (2016). doi:10.1016/j.cell.2016.05.025 Medline

13. Z. Liu, W. R. Legant, B. C. Chen, L. Li, J. B. Grimm, L. D. Lavis, E. Betzig, R. Tjian, 3D imaging of Sox2 enhancer clusters in embryonic stem cells. *Elife* **3**, e04236 (2014). doi:10.7554/eLife.04236 Medline

14. I. I. Cisse, I. Izeddin, S. Z. Causse, L. Boudarene, A. Senecal, L. Muresan, C. Dugast-Darzacq, B. Hajj, M. Dahan, X. Darzacq, Real-time dynamics of RNA polymerase II clustering in live human cells. *Science* **341**, 664–667 (2013). doi:10.1126/science.1239053 Medline

15. W. K. Cho, N. Jayanth, B. P. English, T. Inoue, J. O. Andrews, W. Conway, J. B. Grimm, J. H. Spille, L. D. Lavis, T. Lionnet, I. I. Cisse, RNA polymerase II cluster dynamics predict mRNA output in living cells. *Elife* **5**, e13617 (2016). doi:10.7554/eLife.13617 Medline

16. C. Buecker, R. Srinivasan, Z. Wu, E. Calo, D. Acampora, T. Faial, A. Simeone, M. Tan, T. Swigut, J. Wysocka, Reorganization of enhancer patterns in transition from naive to primed pluripotency. *Cell Stem Cell* **14**, 838–853 (2014). doi:10.1016/j.stem.2014.04.003 Medline

17. J. B. Grimm, B. P. English, J. Chen, J. P. Slaughter, Z. Zhang, A. Revyakin, R. Patel, J. J. Macklin, D. Normanno, R. H. Singer, T. Lionnet, L. D. Lavis, A general method to improve fluorophores for live-cell and single-molecule microscopy. *Nat. Methods* **12**, 244–250, 3, 250 (2015). doi:10.1038/nmeth.3256 Medline

18. P. Filippakopoulos, J. Qi, S. Picaud, Y. Shen, W. B. Smith, O. Fedorov, E. M. Morse, T. Keates, T. T. Hickman, I. Felletar, M. Philpott, S. Munro, M. R. McKeown, Y. Wang, A. L. Christie, N. West, M. J. Cameron, B. Schwartz, T. D. Heightman, N. La Thangue, C. A. French, O. Wiest, A. L. Kung, S. Knapp, J. E. Bradner, Selective inhibition of BET bromodomains. *Nature* **468**, 1067–1073 (2010). doi:10.1038/nature09504 Medline

19. J. Lovén, H. A. Hoke, C. Y. Lin, A. Lau, D. A. Orlando, C. R. Vakoc, J. E. Bradner, T. I. Lee, R. A. Young, Selective inhibition of tumor oncogenes by disruption of super-enhancers. *Cell* **153**, 320–334 (2013). doi:10.1016/j.cell.2013.03.036 Medline

20. N. F. Marshall, D. H. Price, Control of formation of two distinct classes of RNA polymerase II elongation complexes. *Mol. Cell. Biol.* **12**, 2078–2090 (1992). doi:10.1128/MCB.12.5.2078 Medline

21. Y. Shin, C. P. Brangwynne, Liquid phase condensation in cell physiology and disease. *Science* **357**, eaaf4382 (2017). doi:10.1126/science.aaf4382 Medline

22. B. R. Sabari, A. Dall'Agnese, A. Boija, I. A. Klein, E. L. Coffey, K. Shrinivas, B. J. Abraham, N. M. Hannett, A. V. Zamudio, J. C. Manteiga, C. H. Li, Y. E. Guo, D. S. Day, J. Schuijers, E. Vasile, S. Malik, D. Hnisz, T. I. Lee, I. I. Cisse, R. G. Roeder, P. A. Sharp, A. K. Chakraborty, R. A. Young, Coactivator condensation at super-enhancers links phase separation and gene control. *Science* 10.1126/science.aar3958 (2018).

23. B. Gu, T. Swigut, A. Spencley, M. R. Bauer, M. Chung, T. Meyer, J. Wysocka, Transcription-coupled changes in nuclear mobility of mammalian cis-regulatory elements. *Science* **359**, 1050–1055 (2018). doi:10.1126/science.aao3136 Medline

24. J. R. Chubb, S. Boyle, P. Perry, W. A. Bickmore, Chromatin motion is constrained by association with nuclear compartments in human cells. *Curr. Biol.* **12**, 439–445 (2002). doi:10.1016/S0960-9822(02)00695-4 Medline

25. J. S. Lucas, Y. Zhang, O. K. Dudko, C. Murre, 3D trajectories adopted by coding and regulatory DNA elements: First-passage times for genomic interactions. *Cell* **158**, 339–352 (2014). doi:10.1016/j.cell.2014.05.036 Medline

26. V. Dion, S. M. Gasser, Chromatin movement in the maintenance of genome stability. *Cell* **152**, 1355–1364 (2013). doi:10.1016/j.cell.2013.02.010 Medline

27. S. C. Weber, A. J. Spakowitz, J. A. Theriot, Bacterial chromosomal loci move subdiffusively through a viscoelastic cytoplasm. *Phys. Rev. Lett.* **104**, 238102 (2010). doi:10.1103/PhysRevLett.104.238102 Medline

28. E. Bertrand, P. Chartrand, M. Schaefer, S. M. Shenoy, R. H. Singer, R. M. Long, Localization of ASH1 mRNA particles in living yeast. *Mol. Cell* **2**, 437–445 (1998). doi:10.1016/S1097-2765(00)80143-4 Medline

29. W. A. Whyte, D. A. Orlando, D. Hnisz, B. J. Abraham, C. Y. Lin, M. H. Kagey, P. B. Rahl, T. I. Lee, R. A. Young, Master transcription factors and mediator establish super-enhancers at key cell identity genes. *Cell* **153**, 307–319 (2013). doi:10.1016/j.cell.2013.03.035 Medline

30. S. F. Banani, H. O. Lee, A. A. Hyman, M. K. Rosen, Biomolecular condensates: Organizers of cellular biochemistry. *Nat. Rev. Mol. Cell Biol.* **18**, 285–298 (2017). doi:10.1038/nrm.2017.7 Medline

31. D. M. Chudakov, S. Lukyanov, K. A. Lukyanov, Tracking intracellular protein movements using photoswitchable fluorescent proteins PS-CFP2 and Dendra2. *Nat. Protoc.* **2**, 2024–2032 (2007). doi:10.1038/nprot.2007.291 Medline

32. O. Bensaude, Inhibiting eukaryotic transcription: Which compound to choose? How to evaluate its activity? *Transcription* **2**, 103–108 (2011). doi:10.4161/trns.2.3.16172 Medline

33. W. K. Cho, N. Jayanth, S. Mullen, T. H. Tan, Y. J. Jung, I. I. Cissé, Super-resolution imaging of fluorescently labeled, endogenous RNA polymerase II in living cells with CRISPR/Cas9-mediated gene editing. *Sci. Rep.* **6**, 35949 (2016). doi:10.1038/srep35949 Medline

34. A. Sergé, N. Bertaux, H. Rigneault, D. Marguet, Dynamic multiple-target tracing to probe spatiotemporal cartography of cell membranes. *Nat. Methods* **5**, 687–694 (2008). doi:10.1038/nmeth.1233 Medline

35. J. O. Andrews, W. Conway, W. Cho, A. Narayanan, J. Spille, N. Jayanth, T. Inoue, S. Mullen, J. Thaler, I. I. Cissé, qSR: A quantitative super-resolution analysis tool reveals the cell-cycle dependent organization of RNA polymerase I in live human cells. *Sci. Rep.* **8**, 7424 (2018). doi:10.1038/s41598-018-25454-0 Medline

36. M. Ester, H.-P. Kriegel, J. Sander, X. Xu, in *Proceedings of the Second International Conference on Knowledge Discovery and Data Mining*, E. Simoudis, J. Han, U. Fayyad, Eds., Portland, OR, 2 to 4 August 1996 (AAAI Press, 1996), pp. 226-231.

37. X. Darzacq, Y. Shav-Tal, V. de Turris, Y. Brody, S. M. Shenoy, R. D. Phair, R. H. Singer, In vivo dynamics of RNA polymerase II transcription. *Nat. Struct. Mol. Biol.* **14**, 796–806 (2007). doi:10.1038/nsmb1280 Medline

38. T. Lambert, L. Shao, LLSpy v0.3.7. Zenodo (22 November 2017); doi:10.5281/zenodo.1064782.

39. J. Schindelin, I. Arganda-Carreras, E. Frise, V. Kaynig, M. Longair, T. Pietzsch, S. Preibisch, C. Rueden, S. Saalfeld, B. Schmid, J. Y. Tinevez, D. J. White, V. Hartenstein, K. Eliceiri, P. Tomancak, A. Cardona, Fiji: An open-source platform for biological-image analysis. *Nat. Methods* **9**, 676–682 (2012). doi:10.1038/nmeth.2019 Medline

40. C. Y. Jao, A. Salic, Exploring RNA transcription and turnover in vivo by using click chemistry. *Proc. Natl. Acad. Sci. U.S.A.* **105**, 15779–15784 (2008). doi:10.1073/pnas.0808480105 Medline

41. M. Ovesný, P. Křížek, J. Borkovec, Z. Švindrych, G. M. Hagen, ThunderSTORM: A comprehensive ImageJ plug-in for PALM and STORM data analysis and super-resolution imaging. *Bioinformatics* **30**, 2389–2390 (2014). doi:10.1093/bioinformatics/btu202 Medline

42. K. L. Tsai, C. Tomomori-Sato, S. Sato, R. C. Conaway, J. W. Conaway, F. J. Asturias, Subunit architecture and functional modular rearrangements of the transcriptional Mediator complex. *Cell* **158**, 463 (2014). doi:10.1016/j.cell.2014.06.036 Medline

43. S. Sato, C. Tomomori-Sato, C. A. Banks, I. Sorokina, T. J. Parmely, S. E. Kong, J. Jin, Y. Cai, W. S. Lane, C. S. Brower, R. C. Conaway, J. W. Conaway, Identification of mammalian Mediator subunits with similarities to yeast Mediator subunits Srb5, Srb6, Med11, and Rox3. *J. Biol. Chem.* **278**, 15123–15127 (2003). doi:10.1074/jbc.C300054200 Medline